Vânia Alexandra Fernandes Lourenço

Graduated in Chemical and Biochemical Engineering

Evaluation of ecotoxicological properties of industrial wastewater after photocatalytic treatment

This dissertation is submitted to the degree of
Master in Chemical and Biochemical Engineering

Supervisor: María Concepción Ovín Ania, CEMHTI, CNRS, Orleáns, France
Second Supervisor: Isabel Maria de Figueiredo Ligeiro da Fonseca, Univ. Nova de Lisboa, Lisbon, Portugal

Jury:

President: Prof. Dra Maria Madalena Alves Campos de Sousa Dionísio Andrade
Arguing: Prof. Dra Maria Manuel Serrano Bernardo
Vowel: Prof. Dra Isabel Maria de Figueiredo Ligeiro da Fonseca

FACULDADE DE CIÊNCIAS E TECNOLOGIA
UNIVERSIDADE NOVA DE LISBOA

September 2017

Vânia Alexandra Fernandes Lourenço

Graduated in Chemical and Biochemical Engineering

Evaluation of ecotoxicological properties of industrial wastewater after photocatalytic treatment

This dissertation is submitted to the degree of
Master in Chemical and Biochemical Engineering

Supervisor: María Concepción Ovín Ania, CEMHTI, CNRS, Orleáns, France
Second Supervisor: Isabel Maria de Figueiredo Ligeiro da Fonseca, Univ. Nova de Lisboa, Lisbon, Portugal

Jury:

President: Prof. Dra Maria Madalena Alves Campos de Sousa Dionísio Andrade
Arguing: Prof. Dra Maria Manuel Serrano Bernardo
Vowel: Prof. Dra Isabel Maria de Figueiredo Ligeiro da Fonseca

September 2017

Avaliação de propriedades ecotoxicológicas de águas industriais após o tratamento fotocatalítico

Evaluation of ecotoxicological proprieties of industrial waste water after photocatalytic treatment

“Remember Who You Are”

Daisy Wademan

To my big Brother.

AGRADECIMENTOS

Estes seis meses não deram apenas frutos a um nível cientifico, mas também a um nível pessoal. Aprendi como é viver noutro país, viver sozinha e a comunicar diariamente numa língua não materna, foi um enorme processo de crescimento. Mas tudo isto não foi conseguido sem ajuda, a todas as pessoas que se seguem quero dar o meu sincero agradecimento:

Á minha orientadora Doutora Maria Conchi Ania pela sua disponibilidade, compreensão, esclarecimento de duvidas e orientação, mas acima de todo isto, pelos ensinamentos, pois sem a sua ajuda, a realização deste trabalho não seria possível e por fim pela confiança depositada em mim.

Á minha co-orientadora, Doutora Isabel Fonseca, o meu eterno Obrigada, pois toda esta experiencia não teria um final tão maravilhoso sem a sua cooperação, estimulo, prontidão e disponibilidade. A sua ajuda na seleção do tema de dissertação, local e orientação foram cruciais.

Ao *Consejo Superior de Investigaciones Científicas* (CSIC) por autorizar a realização deste trabalho no *Instituto Nacional del Carbón*.

À bolsa atribuída no âmbito do Programa Erasmus+ para realização da mobilidade.

Ao Doutor José Parra por estar sempre disponível a ensinar, partilhar conhecimentos e pela constante boa disposição. Durante o período que estive no INCAR não existiu ninguém mais humano e prestável.

Aos amigos que fiz no final deste percurso por tudo o que me ensinaram sobre as Asturias e o que é ser asturiano. Por escutarem todos os meus 'protestos' (que não foram poucos) e por acreditarem em mim mais do que eu mesma: *Muchas gracias*: Doutora Isabel Alonso-Buenaposada, Doutor Luis Adrián Montoya, Héctor García Álvarez, Doutora Ana Más, Marc Escamilla, Ivan Sainz, Laura Florentino Lopez, Luis Fernández e Rebecca García Valcárcel.

Á Sofia Rebocho e Carolina Nunes por estarem ao meu lado sempre que precisei, por serem as irmãs que não tive, mas pude escolher.

Ao David Liebermann, Tiago Melo, Marta Faria, Duarte Silva, Tiago Alves, Justine Gouvenaux e muitos mais por fazerem o meu percurso universitário memorável.

À Andreia Sousa, minha coordenadora em todos estes anos em que fui trabalhadora estudante, que me flexibilizou horários, férias e licenças sem vencimento para que conseguisse terminar tanto a licenciatura como o mestrado.

Ao Hugo Lourenço, o meu irmão mais velho, porque foi a primeira pessoa a acreditar comigo

neste sonho, apoiou-me e acompanhou-me até ao final: és incansável.

Ao João Beirão, meu cunhado, pela ajuda, pelas palavras encorajamento, amizade e por me aturar diariamente.

Á Helena Fernandes e Pedro Candeias, mãe e padrasto, porque quando precisei estavam lá para contribuir de diferentes formas para este objetivo comum.

Sem querer esquecer toda a família Beirão e Baptista, em especial ao Engenheiro Eduardo Beirão.

Por fim, mas não menos importante, aquele que se tornou um dos meus melhores amigos e companheiro, nestes últimos 7 anos, António Baptista. Porque mesmo quando deixei de acreditar que conseguia mostrou-me que estava errada, porque sem ti nada disto seria possível. Obrigada Xoooni!

RESUMO

A fotocatálise heterogénea é uma das tecnologias mais promissoras para a degradação de poluentes emergentes em corpos hídricos, devido à ampla disponibilidade de fotocatalisadores de baixo custo e de elevada eficiência. O desafio, no entanto, é aumentar a exploração da luz solar através do uso de fotocatalisadores com atividade melhorada sob irradiação solar. A maioria dos estudos sobre este tópico concentra-se no aumento do rendimento da fotodegradação pela incorporação dos aditivos de carbono. No entanto, o impacto do aditivo carbonáceo sobre a toxicidade do efluente final é pouco abordado e pouco se sabe sobre a natureza dos intermediários formados quando se modifica a via da fotooxidação.

Neste contexto, o objetivo deste trabalho foi avaliar o impacto da incorporação de carbonos nanoporosos (como fotocatalisadores ou aditivos para semicondutores) em termos de avaliação de risco da ecotoxicidade usando fenol como poluente orgânico modelo.

Neste trabalho foram utilizados como catalisadores TiO_2, CQ e compósitos de TiO_2/CQ. Foi medida a ecotoxicidade das amostras após 1,3 e 6 horas de fotodegradação para amostras sintéticas de fenol e amostras reais de um efluente de origem industrial.

Os resultados são interpretados em termos de ecotoxicidade das soluções obtidas após os ensaios fotocatalíticos, utilizando a inibição de bioluminescência da bactéria *Vibrio fischeri*, comparando com as características dos componentes de carbono (estrutura, textura) sobre o desempenho dos fotocatalisadores de semicondutores/carbono, usando como semicondutores TiO_2.

Para as amostras de águas sintéticas e reais, os valores de ecotoxicidade mais baixos foram alcançados após 6 horas de fotorradiação com o CQ como catalisador.

Os resultados com amostras reais também mostraram que os ensaios de fotodegradação realizados com catalisadores de carbono nanoporosos/semicondutores híbridos podem ser mais efetivos que os semicondutores isolados ou a fotólise.

Palavras-chave: Ecotoxicidade, fotocatálise, carvão, fenol, TiO_2, *Vibrio fischeri*

ABSTRACT

Heterogeneous photocatalysis is one of the most promising technologies for an advanced degradation of emerging pollutants in water bodies, due to the widespread availability of low-cost and efficient photocatalysts. The challenge, however, is to boost the exploitation of solar light through the use of photocatalysts with improved activity under sun irradiation. Most studies on this topic focus on the enhanced photodegradation yields achieved by the incorporation of the carbon additives. However the impact of the carbonaceous additive on the toxicity of the final effluent is scarcely addressed and little is known on the nature of the intermediates formed when the photooxidation pathway is modified.

In this context, the aim of this work was to evaluate the impact of the incorporation of nanoporous carbons (either as photocatalysts or additives to semiconductors) in terms of an ecotoxicity risk assessment using phenol as a model organic pollutant.

In this work it was used as catalysts TiO_2, CQ and composites of TiO_2 with CQ. It was measured the ecotoxicity of samples after 1, 3 and 6h of photodegradation for synthetic samples of phenol and wastewater from industrial origin.

The results are interpreted in terms of the ecotoxicity of the solutions obtained after the photocatalytic assays by using the bioluminescence inhibition of the bacterium *Vibrio fischeri*, while exploring the role of the carbon component features (i.e. structure, texture) on the performance of the semiconductor/carbon photocatalysts, TiO_2 using semiconductors.

For both synthetic and real wastewater samples the lower ecotoxicity values were achieved after 6 hours of irradiation with the CQ as catalyst.

The results with real samples have also shown that photodegradation assays performed with hybrid semiconductor/nanoporous carbon catalysts can be more effective than the semiconductors alone or photolysis.

Keywords: Ecotoxicity, photocatalysis, carbons, phenol, TiO_2, *Vibrio fischeri*

TABLE OF CONTENTS

LIST OF FIGURES

LIST OF TABLES

LIST OF ABBREVIATIONS

ADPOR – Group of Adsorption and environmental protection on porous solids (www.incar.csic.es/adpor)

AOP - Advanced Oxidation Processes

BC – Before Christ

BET - Brunauer Emmett Teller

CB - Conduction band

CQ – Commercial activated carbon (brand name Aquasorb 2000)

CSIC – Consejo Superior de Investigaciones Científicas

DNA – Deoxyribonucleic acid

DR - Dubinin-Radushkevich

DRS - Diffuse reflectance spectroscopy

EC_{50}- Half maximal effective concentration

Eg - Band gap energy

E-PRTR - European Pollutant Release and Transfer Register

FAO - Food and Agriculture Organization of the United Nations

INCAR - Instituto Nacional del Carbon

IPCC - Intergovernmental Panel on Climate Change

IUPAC - International Union of Pure and Applied Chemistry

LD50 - Median lethal dose

OAS - Osmotic adjustment solution

PRTR-ES - Spanish Pollutant Release and Transfer Register

PZC - Point of zero charge

SECAT - Sociedad Española de Catálisis

SEM - Scanning electron microscopy

SSWM - Sustainable sanitation and water management

TEXP – Time of exposure

UNESCO - United Nations Educational, Scientific and Cultural Organization

UV-Vis - Ultraviolet-visible

VB - Valence band

WWTP - Wastewater treatment plants

XRD - X-Ray diffraction spectroscopy

Chapter

1. Introduction

1.1. Water Pollution

Water, a simple molecule composed of an oxygen atom and two hydrogen atoms linked by a covalent bond, is a colorless/transparent, odorless and tasteless substance essential for all living organisms on Earth. Despite two thirds of the planet are covered by water, freshwater accounts only to a small fraction – about 2.5 % – mostly located in polar icecaps, glaciers and permanent snow Figure 1.1. Thus, less than 0.7 % of freshwater (contained in rivers, lakes and groundwater) can be directly used [Alyssa, 1997], and its availability is strongly dependent on the water cycle -use and sanitation- [Kay, 1999].

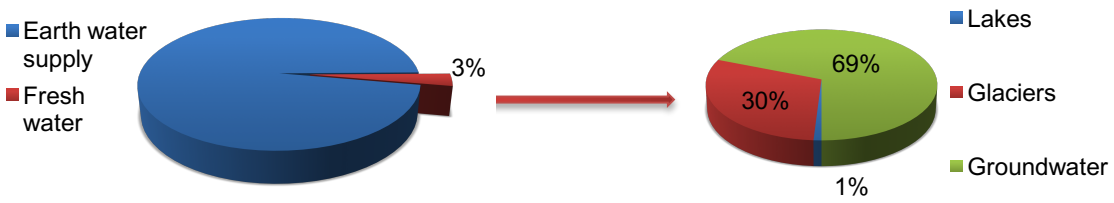

Figure 1.1- Water that covers the planet earth, *adapted from [UNESCO, 2015]*

Water also plays a crucial role in sustaining a high quality of life, with unquestionable impact on human health (on average, an adult body is constituted by ca. 60% of water). The demand for food, drinkable water and industrialization makes water the most used natural resource, followed by oil and natural gas. So, water has a key role in the world economy, aside from being the basis of life [Ruz, 2011].

This natural resource, with no substitute, has become increasingly scarce and rainfall is its ultimate source. In the last 15 to 20 years, non-governmental organizations intensified the awareness about the abusive use of water, but water consumption is still growing every year. According to the Intergovernmental Panel on Climate Change (IPCC) the four main factors responsible for the aggravating water shortage are population growth, the increasing number and size of urban areas in developing countries, overconsumption and climate changes [Spencer, 2010].

Besides these factors, it is important to recall that the demand for water continues to increase at an alarming rate with global consumption, increasing twice as fast as population growth [WWAP, 2009]. According to UNESCO, about 1.2 billion people lack access to safe drinking water, ca. 2.6 billion have little or no sanitation, causing the transmission of lethal diseases through unsafe water or human excreta [Shannon, 2008]. These numbers are expected to increase, for which water will soon become the subject of international conflicts. Indeed, in 2025, the FAO (Food and Agriculture Organization of the United Nations) has estimated that at least 1.8 billion people will be living in regions with severe water scarcity [WWAP, 2015].

1.2. Water world distribution and use

The main uses of water are: domestic supply, breeding of aquatic species, industrial supply, generation of electricity, irrigation, navigation, animal supply, landscape harmony, preservation of aquatic life and dilution and transport of wastes.

Domestic consumption accounts for the smallest fraction of the total water consumption (Figure 1.2), and it is mainly dedicated to clean, cook, and toilet discharges. The biggest waster footprint is the agriculture sector, followed by industry [Sperling, 2007]. The demand of agriculture is also rising rapidly, since the demand for food from the world's population has tripled since the 20th century (Figure 1.3). Additionally, within the next fifty years, the world population is expected to increase by another 40 to 50% [Margaux, 2012], thus contributing to create water tensions.

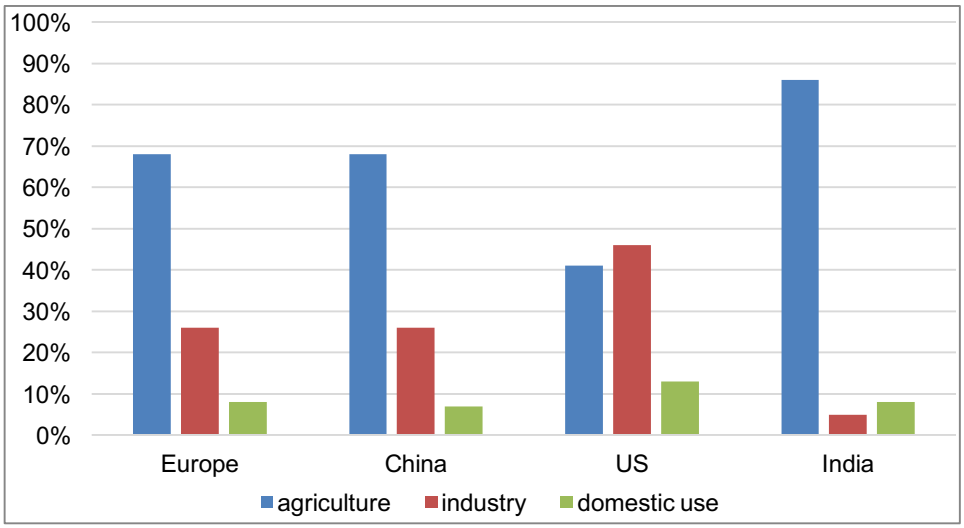

Figure 1.2 – Water consumption distribution by regions and use, *adapted from* [SSWM, 2012]

Furthermore, the consumption of water *per capita* varies significantly among countries and continents, ranging from ca. 10 to approximately 600 L/day [Idowu, 2009; Lips, 2010]. In contrast, 50 L/day is the recommended value to assure basic hygiene and food needs [Allard, 1991; Falkenmark, 2004; Lehr, 2005].

As mentioned before, the industry is the second largest consumer of water, since industrial revolution water is mainly used to produce electricity, cooling systems or as a solvent. These first two activities account for more than 50 % of the total gross water withdrawal (i.e., taken from source), surface and groundwater, in most EU countries. Figure 1.3 also shows that the amount of water withdrawal by the industry remained almost unchanged since mid-80's, demonstrating that the concept of water recycling within factory's processes is viable [WWAP, 2017].

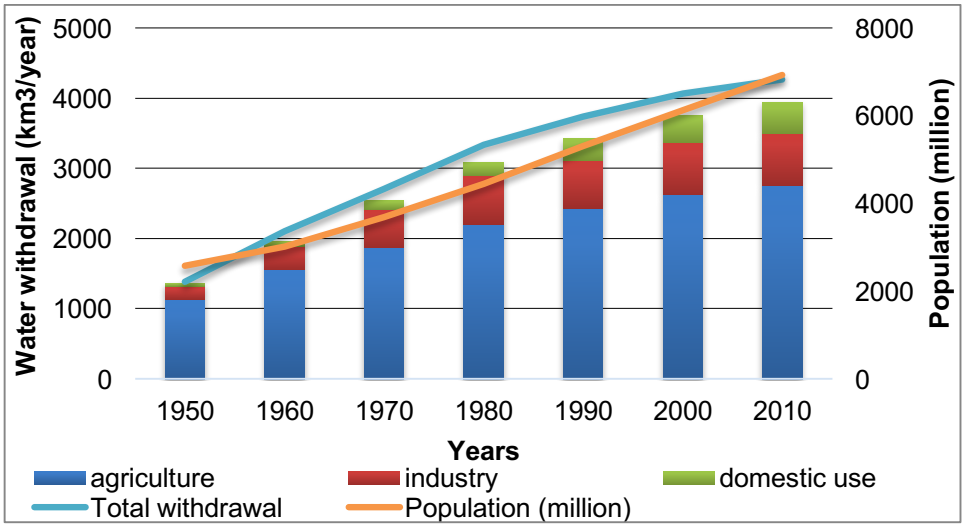

Figure 1.3 – Global population and water withdrawal over time, *adapted from [AQUASTAT, 2016]*

The amount of water used for construction and other industrial activities also varies significantly between countries. As shown in Table 1.1, the highest values of water consumption *per capita* are used for the production of electricity, and other manufacturing processes. However, it is important to point out that the amount and quality of water needed in industry depend on the nature of the activity itself and the technological processes applied.

Table 1.1 - Total water abstraction, share of surface water abstraction, by activity. Data since 2006 to 2011, *adapted from* [Whelminger, 2014]

	Manufacturing industry		**Production of electricity - Cooling**	
	Total water abstraction (m^3/inhabitant)	Share of surface water abstraction (%)	Total water abstraction (m^3/inhabitant)	Share of surface water abstraction (%)
Belgium	101.3	93.9	380.2	100
Bulgaria	18.5	46.8	512.5	99.9
Czech Republic	22.3	89	65	100
Denmark	6	0.3	0.3	0
Germany	57	83.6	243.8	
Estonia	15.7	71.4	757.8	100
Greece			9	73.3
Spain	10.9	65.1	135.5	100
France	41.2	60.3	339.1	99.9
Croatia	7.4	74.5	27.2	99.1
Latvia	11.1	44.9	1	86
Lithuania	9.3	86	87.8	100
Hungary	8.1	48.5	432.9	99
Netherlands	186.9	95.1	343.7	99.9
Poland	12.3	66.5	178.8	99.8
Romania	36.6	84.9	165.5	99.7

1.3. Water quality

Water treatment technology has been identified as a high priority research area due to the overwhelming impacts of water scarcity, lack of adequate sanitation systems in human needs, and lately, the fear generated upon the possibility of water contamination. Consequently, the need for the development of smart and integrated response strategies to guarantee water quality protection against current threats is most urgent.

Historically, the answer to water scarcity has been boosting new sources of water supply however, this strategy no longer guarantees the water security and Europe must look at new tactics, such as water conservation, water-use efficiency improvements and water recycling. Special attention is nowadays being paid to the reutilization of poor quality water, including treated wastewater -already used for irrigation purposes in some countries-. However, the implementation of wastewater reuse in Europe faces quite a few challenges, related to the presence of pollutants, the low coverage of water sanitation and low social acceptance. If this strategy is to be extended for human consumption resources, a precise control of water quality is essential. In this regard, the quality of water and treated water is different depending on the end-user and/or reutilization purposes.

Table 1.2 presents water general and specific uses as well as the main quality requirements for each use [Sperling, 2007]. As seen, domestic water supply is the most demanding sector that requires the fulfillment of several quality standards. In the case of water bodies with multiple uses, the final quality must also satisfy multiple requirements. It should also be pointed out that reaching zero levels of certain contaminants may not be feasible (or even necessary), for certain final reutilization proposes.

Besides domestic effluents, the dawn of the industrial revolution in the eighteenth century in the now developed countries pointed out the beginning of society's dilemma with the fate of wastewaters originated from industrial activities [WWAP, 2017]. Then and now, industrial effluents have been discharged into natural streams (rivers, lakes), with the misguided belief that 'the solution to pollution is dilution'.

An additional challenge is the fact that quality of industrial watercourses is completely dependent of the nature and size of the industry and manufacturing process, and little is known about the pool of pollutants for different processes. To overcome this issue, some developed countries have started to compile and make accessible solid information about wastewater volumes and toxicity.

The European Pollutant Release and Transfer Register (E-PRTR) is the Europe-wide register that provides information about key environmental data from industrial facilities in European Union Member States and associated countries. The database contains details about more than 30,000 industrial facilities, covering over 65 economic activities across Europe [E-PRTR, 2015].

Table 1.2 - Association between water use and quality requirements, *adapted from* [Sperling, 2007].

General USE	**Specific USE**	**Quality requirements**
Domestic supply	-	- Free from chemical substances and organisms harmful to health - Low aggressiveness and hardness - Aesthetically pleasant (low turbidity, color, taste and odor; absence of macro-organisms)
Industrial supply	Water incorporated into the product (e.g. food, drinks, medicines)	- Free from chemical substances and organisms harmful to health - Aesthetically pleasant (low turbidity. color. taste and odor; absence of macro-organisms)
	Water that enters in contact with product	- Variable with the product
	Water that does not enter in contact with product (e.g. refrigeration units, boilers)	- Low hardness - Low aggressiveness
Irrigation	Horticulture. products ingested raw or with skin	- Free from chemical substances and organisms harmful to health - Non-excessive salinity
Animal water supply	-	- Free from chemical substances and organisms harmful to animal's health
Preservation of aquatic supply	-	- Variable with the environmental requirements of the aquatic species to be preserved
Recreation and leisure	Direct contact with liquid medium: e.g. bathing, swimming, water-skiing, surfing	- Free from chemical substances and organisms harmful to health - Low levels of suspended solids, oils and grease.
Transport	-	- Low presence of course material that could be dangerous to vessels
Energy generation	Hydroelectric power plants	- Low aggressiveness
	Nuclear or thermoelectric power plants (e.g. cooling towers)	- Low hardness

Table 1.3 compiles selected pollutants usually present on industrial wastewater, along with their corresponding sources. Other examples of toxic organic pollutants in industrial effluents are: methyl chloride, 1,1,1-trichloroethane, toluene, ethyl benzene, trichloroethylene, tetrachloroethylene, chloroform, bis-2-ethyl-hexyl phthalate, 2,4-dimethyl phenol, naphthalene, butylbenzylphthalate, acrolein, xylene, cresol, acetophenone, methyl-sobutyl-acetone, diphenylamine, aniline and ethyl acetate, among most representatives [Sperling, 2007].

Table 1.3 - Substances present in industrial effluents *adapted from Bond R.G. and Straub C.P.1974* [Sperling, 2007; Pérez, 2014; WWAP, 2017]

Substances	***Source***
Ammonia	Gas. coke and chemical manufacture
Cyanides	Gas and coke manufacture. plating and metal cleaning
Formaldehyde	Synthetic resins and penicillin manufacture
Organic acids	Distilleries and fermentation plants
Phenols	Gas and coke manufacture, chemical plants, textile
Sulfides	Textile industry. tanneries and gas manufacture
Zinc	Galvanizing zinc planting and rubber process

1.4. Phenol as a contaminant

Phenol is the parent substance of a homologous series of compounds containing a hydroxyl group bound directly to an aromatic ring, being the simplest aromatic member of alcohol. From a chemical point of view, the hydroxyl group of phenol determines its acidity whereas the benzene ring characterizes its basicity. It is a clear, colorless compound in the molten state, with a low melting point and characteristic odor. Phenol is quite soluble in water and most organic solvents (aromatic hydrocarbons, alcohols, ketones, ethers, acids, halogenated).

Known to be one of the most versatile organic chemicals, phenol has achieved considerable importance as the starting material for numerous intermediates and final products. Until World War II, it was essentially produced by extraction of natural resources (coal-tar and lignin). Because its consumption rose significantly, the extractive methods were replaced by synthetic methods such as the low-temperature carbonization of wood, and the Hock process starting from cumene. It is also formed during petroleum cracking.

Phenol was first used as a disinfectant for sterilizing wounds, surgical dressings and instruments, and household antiseptic. However, it has limited use in pharmaceuticals or household applications due to its toxicity, well documented in the literature. It is known to cause skin caustic burns, dyspnea, cyanosis, lung edema, severe damage to inner organs (kidneys, liver, spleen, lungs) [Rappoport, 2003; Zazo, 2006]. According to some reports [Baruah, 2011], phenol has cytotoxic effect on skeletal muscle, and his derivatives also cause inhibition of DNA synthesis in the human cells, inducing of gene mutations. The LD_{50} of phenol is 1g/L for humans.

Phenol is presented in wastewaters from pharmaceutical, chemical and paper mills with concentrations ranging between 35 and 400 mg/L. It may be also generated from the natural degradation of organic wastes including benzene [Germán, 2009]. In some extreme cases, such as in wastewater from petrochemical, it can reach values of 30 to 50 g/L [Olguin-Lora, 2003].

Figure 1.4 shows data corresponding to the discharge of phenol (and derivatives) to water bodies in Europe, with UK, Norway, Spain and France as main contributors. Among activities, the production of energy (645 t/discharged) and the mineral industry (236 t/discharged) are most polluting sectors, according to the E-PRTR database [E-PRTR, 2015].

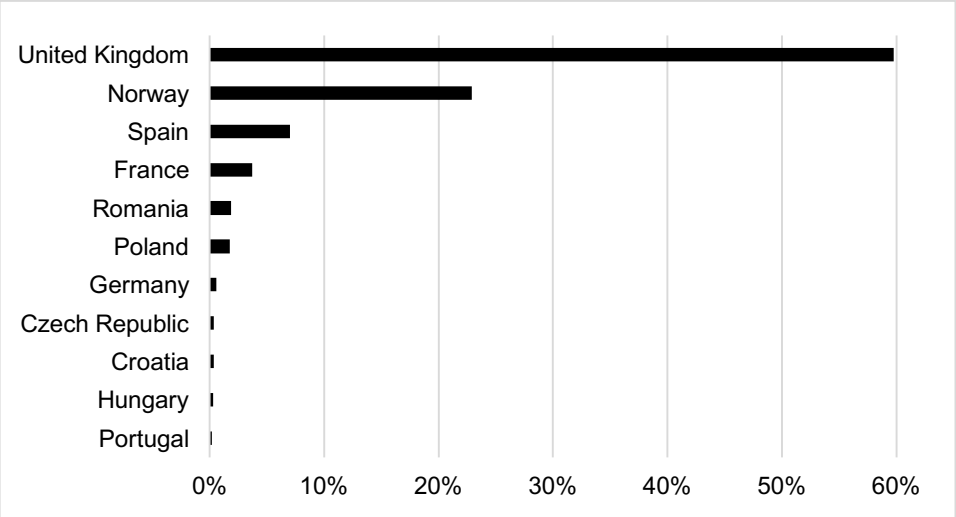

Figure 1.4 - Emissions corresponding to phenol discharges to water bodies in Europe *adapted from [E-PRTR, 2015]*

In Spain, the Spanish Pollutant Release and Transfer Register (PRTR-ES) reported 82 t/discharged in 2015 (of which 5 t accidental), most of them associated to the energy sector and to accidental spills from urban wastewater treatment plants (WWTP) and the Catalonia Region ranked 1st polluting area in Spain (Figure 1.5), in 2015 [PRTR-ES, 2015].

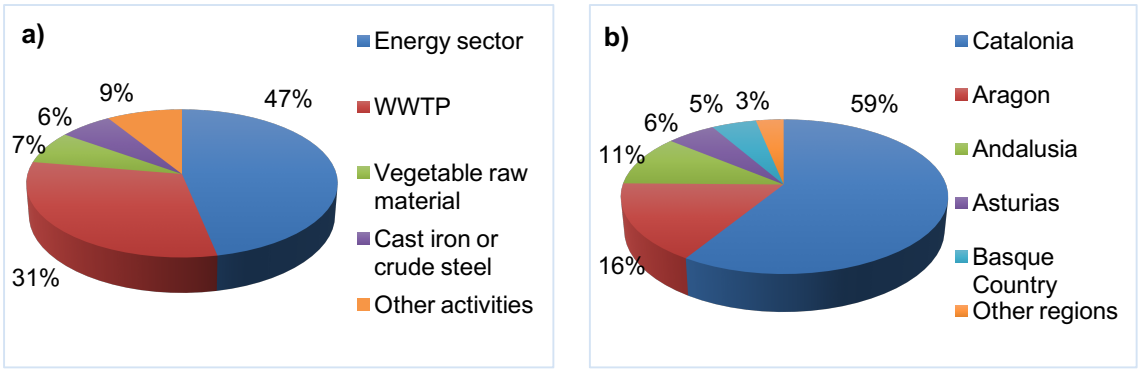

Figure 1.5 - Phenol Discharge to water in Spain, data of 2015 adapted from [PRTR-ES, 2015] a) main polluting sectors and b) main geographical areas

Such high concentrations of phenol in industrial wastewater make the treatment with biological processes non-viable, as it is also known to inhibit the microorganisms activity [Germán, 2009]. Phenol is fast degraded on air, 14.6 hours, by a radical reaction, but may persist in water for a longer period [Crawford, 2006]. Researchers have been using many technologies for phenolic wastewater treatment, such as biological treatment, chemical precipitation or oxidation, ion exchange, adsorption on activated carbons, among others [Khehra, 2006; Zazo, 2006; Lucas, 2007; Raghu, 2007; Wongsarivej, 2009]. Among different alternatives, Advanced Oxidation Processes (AOP) and particularly heterogeneous photocatalysis based on semiconductors has been widely studied for the degradation of phenol and derivatives from water streams.

1.5. Water Treatment Technologies

For millennia, wastewater has been managed in many ways, but still evolving and it's believed to be a non-stopping development. In the past, the first 'sewers' were created in the seventh century BC, in Rome. Around the second and first centuries BC, that same sewers, had an additional system becoming the most complex among the many wastewater collectors at the time. First it was built as an open freshwater canal and second modified into a monumental underground tunnel, with tuff and vaults. Besides the first sewers, Romans were also pioneers on the creation of an economic system around the sanitation services. To use the public latrines or rent chamber pots, it was charged a small fee to keep and expand the sanitation services. Although it is not exactly the same, but these systems (sewage and economic) aren't so different from what is used today [Biscarini, 2017].

Nowadays water treatment varies a lot worldwide, but before the water is re-used or discharged, it generally involves, two or three stages [Wilson, 2016]:

- *Primary Treatment:* removal of solids using filters, screens, sedimentation tanks and dissolved air flotation tanks;
- *Secondary:* biological treatment to remove dissolved organic matter through techniques such as an aeration tank, trickling filter and activated sludge process, followed by settling tanks;
- *Tertiary (advanced treatment):* Additional treatment to remove nutrients, such as nitrogen, phosphorous and suspended solids, through technologies including sand filtration or membrane filtration. Disinfection is often the final step before discharge.

Tertiary treatments are less implemented, although the purpose of these final treatments is to further improve the effluent quality before its discharge to sensitive or fragile receiving environments. Tertiary treatments gather different technologies, and usually involve disinfection with ultraviolet radiation, ozone or chlorine and/or advanced water treatment technologies, as is the case of activated carbons adsorption and AOPs. The effluents from a tertiary treatment may be sufficiently clean to become a reclaimed water source which may be reused.

1.5.1. Heterogeneous Photocatalysis

Heterogeneous photocatalysis has become one of the most popular and promising AOP for the degradation of recalcitrant pollutants in air, water and wastewater. Photocatalysis is defined as a change in the rate of a chemical reaction or its initiation under the action of ultraviolet, visible or infrared radiation in the presence of a substance −the photocatalyst− that absorbs light and is involved in the chemical transformation of the reaction partners [Braslavsky, 2007]. The incident light acts as an activating or promoting agent in the reaction, but not as catalyst since it is consumed during the process.

Most commonly used photocatalysts are semiconductors; materials that are able to absorb light irradiation and photogenerate electron/hole (e-/h+) pairs when irradiated with an optimal wavelength. A characteristic feature of semiconductors is the separation of the electron energy levels into two

bands (Figure 1.6): occupied energy states that corresponds to the valence band (VB, upper edge), whereas the unoccupied energy level is the conduction band (CB, lower edge). The difference between those two levels is known as the energy band gap Eg of the semiconductor.

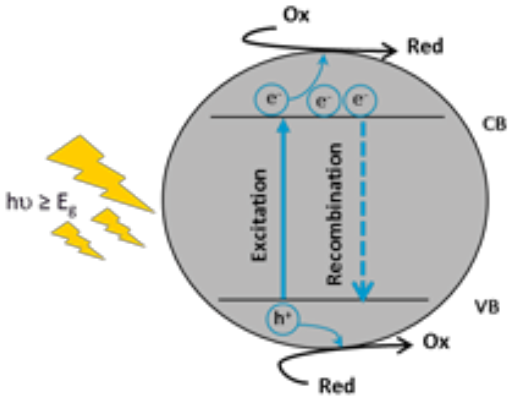

Figure 1.6 - Scheme of the mechanism for n-type semiconductor, *adapted from [Pelizzetti, 1989].*

The mechanism of light absorption in a wide band gap n-type semiconductor −such as titanium dioxide− is based on interband electron transitions between the VB and the CB that may generate a series of chain oxidative-reduction reactions. When semiconductor particles are irradiated with photons with energy equal to or higher than its band gap, electrons (e-) are excited from the VB into the unoccupied CB, whereas positive holes (h+) are created in the VB (reaction 1.1). The photogenerated charge carriers (e-/h+) can recombine radiatively (photoluminescence) or non-radiatively (dissipating the energy as heat), or migrate to the surface reaction sites and get scavenged to react with electron donors or acceptors near the photocatalyst surface (typically water and/or oxygen). The competition between these processes determines the overall efficiency of the photocatalytic process. Subsequent chemical events at the liquid-semiconductor interface between e^-/h^+ pairs and species in solution also determine the efficiency of the photocatalytic reaction. In the case of TiO_2, most common reactions involve the formation of radicals (hydroxyl radicals, superoxide) according to:

$$\text{Semiconductor} + h\nu \longrightarrow e^- + h^+ \qquad \text{(reaction 1.1)}$$

$$H_2O + h^+ \longrightarrow HO^\bullet + H^+ \qquad \text{(reaction 1.2)}$$

$$O_2 + e^- \longrightarrow O_2^{\bullet -} \qquad \text{(reaction 1.3)}$$

The major drawback of most semiconductors is their low photonic efficiency under sunlight. As an example, the benchmark material, TiO_2, does not absorb photons with wavelength longer than 387 nm (i.e. 3.2 eV), thus the sunlight exploitation is reduced to ca. 4 %. Other limitations that have prevented the large-scale implementation of this technology in water treatment are associated to the recovery and reuse of the nanosized TiO_2 powders, and the low surface area of the photocatalysts.

1.5.2. The use of nanoporous carbons in photocatalysis

Triggered by the rising interest in heterogeneous photocatalysis for environmental remediation or energy conversion, numerous approaches have been established to improve the photocatalytic activity of semiconductors. Most approaches focus on the development of new materials with improved activity in the visible region [Malinkiewicz, 2013; Green, 2014; Stranks, 2015], the incorporation of metallic dopants to modify the band gap of the semiconductor, surface sensitization, and the immobilization of the photoactive material on appropriate substrates [Minero, 2000; Cho, 2001; Han, 2009; Maçaira, 2013; Cordero-Garcia, 2016].

Extensive work has also been carried out on the use of carbon materials for this purpose, particularly on the use of different forms of carbons as additives to semiconductors for enhancing the spectral response in the UV and visible light range [Matos, 1998; Tryba, 2008; Faria, 2009; Matos, 2010; Leary, 2011]. Enhancement of the photocatalytic response of such carbon/semiconductor composites has been traditionally attributed to either the strong interfacial electronic effects provided by the carbon matrix, and/or improved mass transfer effects when nanoporous carbons are used as non-photoactive supports.

In 2010, the pioneering studies carried out in the ADPOR group of Dr. Ania (supervisor of this master thesis) have reported the self-photochemical activity of nanoporous carbons under UV-Vis irradiation in the absence of semiconductors [Velasco, 2010]. These studies showed an improvement in photo-oxidation of phenol in aqueous solution by irradiation of an nanoporous carbon (compared to both the photolytic breakdown and the use of either bare or carbon-immobilized titania), demonstrating the effect of the carbon material beyond the synergistic effect of the porosity [Andrade, 2015; Carmona, 2015, 2016; Gomis-Berenguer, 2016].

The combination of photocatalytic runs with electronic spin resonance spectroscopy and electrochemical tools demonstrated the ability of theses nanoporous carbons to generate radical species when irradiated in aqueous environments -although this was not an intrinsic property of all carbon materials- [Velasco, 2013; Velasco, 2014; Gomis-Berenguer, 2017]. As a result, the photodegradation of the target pollutant was enhanced due to the photochemical activity of the nanoporous carbons when irradiated alone, or to its contribution when using semiconductor/nanoporous carbon hybrid photocalysts [Velasco, 2012; Andrade, 2014; Gomis-Berenguer, 2016].

1.6. Ecotoxicity

Toxicity measurement of wastewater, sediments, and contaminated water bodies is a very important part of environmental pollution monitoring. Commonly, various chemical parameters are used for pollution monitoring, such as dissolved oxygen, chemical oxygen demand, total carbon content, total conversion and so forth. However these analyses only indicate the nature of the pollutants or the efficiency of the treatment applied for their removal, and do not yield any information about the biological effects of the remaining species in the waters. Evaluation of biological effects can provide

specific information on toxicity and ecotoxicity, allowing the incorporation of toxicity parameters in environmental regulation.

Paracelsus told us: *Sola dosis facit venenum*, meaning that all things are toxic and the dosage makes it "toxicant". In this context, Gallo in 1995, reinforced by asking two questions: what is it? And how much? In other words, that a toxicant must be defined both qualitatively and quantitatively.

The term ecotoxicology was introduced by René Truhaut in 1969, and reflects the concern about the chemical effects on the environment and in non-human species. Nowadays is defined as the study of the adverse effects of chemicals on ecosystems [Klaassen, 2012; Walker, 2012]. Toxicological bioassays were based upon an experimental design of five elements: the sample, the biota, the duration, the endpoint, and the dose response [Wells, 1998]. The most usual measurement is the endpoint which is usually the death of the biota. The main goal is the use of more sophisticated indices, avoiding death [Walker, 2012].

Various terms are used depending on the exposure time between the organism and the chemical agent. Acute exposure refers to organisms are exposed to a chemical agent in a single event or in multiple events occurring in a short period of time, usually ranging from hours to days. In contrast, chronic exposure refers to organisms exposed to low concentrations of a toxic agent released continuously or with some periodicity over a long period of time (weeks, months or years).

Many methods have been development over the years to monitor and assess the toxicity of the pollutants discharged to water bodies. Traditionally, crustaceans, fish and algae were used for aquatic toxicity measurement, but the tests based on microorganisms have been gaining popularity in the last decades. Animal and plant bioassays typically have good sensitivity and permit real-time analysis. Their main disadvantages are associated to standardization issues of the organisms, the requirement of special equipment and skilled operators, and the lack of reproducibility of the bioassays. On the other hand, bacterial bioassays are rapid, cost effective and more reproducible [Gomes, 2007].

Furthermore, since the 90's, acute toxicity tests for fish and crustacean (daphnia), algae and bacterial growth inhibition have become mandatory tests for the identification of the potential toxicity of substances, according to Europe Union regulations. Some countries, like Denmark, are more demanding and request toxicity tests with five different species: green algae (Rhaphidocellis subcapitata), Daphnia magna, zebrafish (Brachydaniorerio), macrophyte (Lemna minor) and luminescent bacterium (*Vibrio fisheri*). It has been shown in the literature that different organisms react differently to the same compound, so assay methods should be able to reach the actual conditions of the ecosystem. Another challenge of aquatic toxicity testing is related to the changes in the chemical concentration due to the occurrence of absorption and metabolization by the test organism, volatilization and degradation.

1.6.1. Bioluminescence inhibition assays

Bacterial bioassays are thus among most widely used test for evaluating the ecotoxicity, either based on bacteria population growth, substrate consumption, respiration, luminescence or bioluminescence inhibition assays. The growing interest in bacterial bioassays, and particularly bioluminescence one, is due to the fact that, despite the existence of different toxicity mechanisms for various organisms of different species, a substance that is toxic for an organism often demonstrates similar toxic effects on other organisms [Kaiser, 1998]. Thus, luminescence inhibition in bacteria may also indicate toxic effects on higher organisms. The test species used for bioluminescence inhibition assay includes mainly *Vibrio fischeri/Photobacterium phosphoreum*, Vibrio harveyi and Pseudomonas fluorescens.

Among bacterial bioassays, *Vibrio fischeri* luminescence inhibition test is the most common one. *Vibrio fischeri,* is a marine gram negative non-pathogenic bacterium belonging to the Vibrionaceae family, that poses a flexible metabolism [Gomes, 2007]. Several commercial test kits (i.e., Microtox, LUMIStox, ToxAlert) are available in the market [Parveza, 2006].

The reaction is based on the luminescence decay of this bacterium when it is exposed to a chemical agent. The bioluminescence is directly proportional to the metabolic activity of the bacterial population, thus any inhibition of enzymatic activity corresponding to a lethal or sub-lethal response results in a decrease in the bioluminescence signal. The protocol for the measurement of the toxicity has been reported by [Kahru, 1996], and consists basically on exposing a culture suspension with a certain volume of the test chemical agent in an inert electrolyte (typically NaCl) at controlled temperature (ca. near ambient condition) and measure the decrease in the bacterial luminescence due to presence of the toxic compound after a certain time of exposure. The concentration of the pollutant that causes a 50% reduction in light after exposure is designated as the EC_{50}.

Several factors may influence the toxicity and endpoint during the bioassay, such as pH, turbidity, exposure and aging times, and incubation temperature. For instance, solution pH is usually controlled between 6-8 in standardized analysis methods (even although the *vibrio fishery* can live between pH 4-9) to assure reproducibility. As for the exposure time, based on the literature *Vibrio fischeri* inhibition test requires only 5–30 min for toxicity prediction. However, this parameter strongly depends on the substance being tested, thus it is important to optimize it. Another parameter to be considering are the aging of the sample itself, and the fact that *Vibrio fischeri* bacteria are commercialized in a lyophilized state, so need to be reconstituted for its use. Reconstituted bacteria should be used within the next three hours (as the results may be compromised afterwards).

The main advantages and disadvantages associated to the use of *Vibrio fischeri* luminescence inhibition test for the determination of ecotoxicity parameters are shown in Table 1.4.

Table 1.4 - Disadvantages versus advantages of Microtox [Gaudet, 1994; AZUR Environmental, 1998; Blaise, 2005; ModerWater, 2012]

Advantages	**Disadvantages**
- does not take up much laboratory space	-marine bacteria may have little biological significance
- does not require high skilled workers	- the need to increase the salinity of some samples to a level compatible with the requirements of the bacteria used, which may favor the precipitation of heavy metals
- it is a low cost, simple and reproducible method	-bioluminescence of bacteria decreases over time, requiring precise control over the duration of the test (thus limiting the number of samples processed simultaneously)
- it only requires 2.0 ml of sample and the bacteria are easy to obtain and store	- the color and turbidity of the effluent to be tested influences the extent of light emitted.
- variety of solid and liquid samples can be tested, including turbid and colored substances, and the quick response to that vast number of substances;	
- can be used as an early warning system detecting toxins in an aquatic environment	

1.6.2. Phenol ecotoxicity

Phenol is a high toxic pollutant frequently found in wastewaters of various origins, thus its ecotoxicity in aquatic environments has been widely reported in the literature for various species. Table 1.5 collects data corresponding to values of EC_{50} after 5 and 15 min using the *Vibrio fischeri* luminescence inhibition test. Values showed quite a large variability, with $EC_{50\text{-}5'}$ ranging between 10-35.8 mg/L.

Phenol degradation has also been extensively studied, and most common oxidation pathways are quite well-known [Santos, 2002; Nadolna, 2012]. Consequently, the ecotoxicity of its degradation intermediates has also been investigated. Among them, aromatic polyhydroxylated intermediates (such as catechol, hydroquinone, *p*-benzoquinone and resorcinol) display much higher toxicity than phenol itself, as illustrated in Table 1.5.

Table 1.5 – Ecotoxicity of phenolic compounds reported in the literature [Blum, 1991; Boyd, 1997; Hoeben, 2000; Santos, 2004; Merck, 2010; Bendary, 2013].

	$EC_{50\ -5`(mg/L)}$	$EC_{50\ -15`(mg/L}$
Phenol	10-30	20
	20	25.61
	17	21.36
	20.19	21
	13-26	
	21.1-35.8	
	15.1	
Catechol	32	7
		8.32
		2.7
Hydroquinone	0.079	0.04
	0.042	0.041
Resorcinol	375	265 (30 min)
	310	264 (30 min)
	370	
Benzoquinone	0.0085	<0.01
	0.020	
	0.08	
	1.4	

Chapter

2. Objective

Objective

The main goal of this master thesis was to evaluate the impact of the incorporation of nanoporous carbons (either as photocatalysts or additives to semiconductors) on the ecotoxicological properties of the treated water after the photocatalytic treatment, using phenol as a model organic pollutant commonly present in industrial wastewaters. The specific objectives followed to achieve the main purpose of this thesis were:

- To optimize and validate an experimental protocol based on the inhibition luminescence of *Vibrio Fisheri* bacterium for the evaluation of the ecotoxicity of synthetic aqueous solutions containing phenolic derivatives, as well as in real wastewater from industrial origin.
- To analyze the ecotoxicity of solutions after photocatalytic degradation using TiO_2 nanopowders as benchmark photocatalyst using simulated solar light.
- To analyze the ecotoxicity of solutions after photocatalytic degradation using a nanoporous carbon either as photocatalyst or additive to TiO_2, using simulated solar light.

The research described in this master thesis has been performed in Oviedo, Spain, within a research internship in the framework of the Eramus+ Program agreement reference PLISBOA03 between Universidad Nova de Lisboa in Portugal and Universidad de Oviedo in Spain. The activities of the internship were carried out at Instituto Nacional del Carbon (INCAR, belonging to Agencia Estatal CSIC) in Oviedo, under the supervision of Dr. Ania (Tenured Scientist of CSIC in Spain -currently in absence leave-, and Directeur de Recherche of CNRS in France -current affiliation-) according to the agreement Universidad de Oviedo-CSIC for education and scientific activities (BOPA núm. 139 de 17-vi-2013).

The results obtained so far in this master thesis have been presented in a poster communication at the conference SECAT (see details below):

Lourenço V (presenter), García-González R, Parra JB, Fonseca IM, Gomis-Berenguer A, Ania CO, Ecotoxicity assessment of the photocatalytic performance of semiconductor/nanoporous carbon photocatalysts, Congreso de la Sociedad Española de Catálisis SECAT-2017, 25-28 June 2017, Oviedo, Spain (poster communication).

Objective

Chapter

3. Experimental

3.1. Materials

3.1.1. Semiconductors

Commercially available titanium dioxide powders manufactured by Degussa (Evonik, brand name P25) were selected as semiconductor. This material is widely used both in academia and industry, and has become a benchmark for photocatalytic applications.

We have selected a commercial activated carbon (CQ) (supplier Agrovin SA, Spain; brand name Aquasorb 2000) obtained from the physical activation of bituminous coal with CO_2. A particle size of 0.212-0.710 mm was selected for all the experiments. Before usage, the carbon was washed in distilled water at 60 ºC, dried at 110 ºC overnight and kept in a desiccator until use. This carbon is characterized by low oxygen content (ca. 2.1 wt.%), a basic nature (point of zero charge of 9.2 pH units).

For the preparation of the composites, a weight ratio of 10% was selected based on our previous studies [Haro, 2012]. The semiconductor/carbon composites were prepared by physical mixture of commercial titanium oxide (P25) and the activated carbon in a mortar.

3.1.2. Pollutants

Synthetic solutions were made using phenol, catechol, resorcinol, hydroquinone and benzoquinone (purity at least 99 % Sigma-Aldrich and Merck reactives). Initial concentration of the synthetic solutions was ca. 100 ppm. Precautions need to be taken during the preparation of phenolic solution (particularly during weighting) since phenol liquefies fast when exposed to air, and reacts with plastic holder (thus glass holders were used). The prepared synthetic solutions were stored in dark containers and at low temperature (≈4ºC).

A real wastewater sample was used in this study. Before the analysis of the real wastewater, it was stirred for 15 minutes and filtered (filter pore size ca. 8 μm). Selected physicochemical parameters of the real wastewater are in Table 3.1.

Table 3.1 -physicochemical parameters of the real wastewater

Parameters		**Units**
pH	8.6	--
conductivity	1067	microS/cm at 20ºC
suspended solids	39	mg/L
Chemical Oxygen Demand	848	mg/L
Total organic Carbon	291	mg/L
Phenols	4.2	mg/L
Total Hydrocarbons	2.2	mg/L

3.2. Characterization

3.2.1. Textural characterization

The International Union of Pure and Applied Chemistry (IUPAC) defines the texture of a material as the detailed geometry of the void and pore space [Sing, 1985; Thommes, 2015]. Porosity is a concept related to texture and may be defined as the ratio between the volume of pores and voids, and the volume occupied by the solid. However, given porosity value cannot be regarded as characteristic of the material, since it depends on the method used for its determination. The accessible area of solids increases with the splitting state of the solid, but mainly depends on the porosity of the surface. In a way that is necessarily arbitrary, it is considered that the outer area corresponds to the area of the walls of the pores and slits having a depth greater than the width. Porous solids usually have an internal area that is of a much higher order of magnitude than the external area.

IUPAC classifies the pores according to their size as [Sing, 1985; Thommes, 2015]:

i) *Macropores*: pore widths, exceeding about 50 nm;
ii) *Mesopores*: pore widths between 2 nm and 50 nm;
iii) *Micropores*: pore widths not exceeding about 2 nm.

More recently, the term *nanopores* was accepted to include the above three categories of pores, but with an upper limit close to 100 nm width [Thommes, 2015]. Some other authors proposed additional classifications to distinguish, for instance, *ultramicropores* with less than 0.7 nm; *micropores*, corresponding to a widths between 0.7 and 1.4 nm; and *supermicropores*, widths between 1.4 and 3.4 nm [Rouquerol, 2014].

In this experiment the nanoporous texture of the materials has been characterized by physical adsorption of different gases, obtaining different parameters such as specific surface area, total volume of pores and pore size distribution. Two volumetric analyzers were used for N_2 isotherms at -196 °C: ASAP 2020 and TRISTAR 3020, both supplied by Micromeritics. All samples were previously outgassed under vacuum (ca. 10^{-1} Pa) at 120 °C (heating rate of 2.5 °C/min) for 17 h, following the recommended conditions to obtained reproducible and accurate data [Figini-Albisetti, 2010]. Dubinin-Radushkevich (DR) equation has been applied to the N_2 adsorption isotherms at -196 °C to obtain the total micropore volume (Wo, N_2).

3.2.2. Adsorption of gases

Adsorption is a spontaneous process that occurs when the surface of a solid is exposed to a gas or a liquid. More specifically, it can be defined as the enrichment of molecules, atoms or ions in the vicinity of an interface. According to the nature of the interactions, a distinction can be made between physical adsorption (or physisorption) and chemical adsorption (or chemisorption). The amount of gas adsorbed, n, per mass of solid depends on the pressure, p, the temperature, T, and the nature of the

gas-solid system. For a given gas adsorbed on a particular solid at a constant temperature, and if the gas is below its critical temperature, the number of moles of gas adsorbed may be expressed as:

$$n = f\left(\frac{p}{p_0}\right)_{T,gas,solid} \qquad \text{Equation 3.1}$$

Where p_0 is the gas saturation pressure and p/p_0 is the relative pressure.

This equation is a general expression for an adsorption isotherm and represents the relationship between the amount adsorbed by unit mass of solid and the equilibrium pressure (or relative pressure), at a known temperature.

Experimental adsorption isotherms are usually presented in graphical form, and display various characteristic shapes for many different gas-solid systems. These shapes are important since they provide useful preliminary information about the pore structure of the adsorbent. The majority of gas/ vapor adsorption isotherms (i.e. at subcritical temperatures) may be divided into six groups (I to VI), according to the extended IUPAC classification proposed in 2015 [Thommes, 2015] (see Figure 3.1). Others can usually be explained as a combination of two (or more) of the shapes proposed (composite or hybrid isotherms). The six Types I, II, III, IV, V and VI are similar to those originally proposed by Brunauer, Deming, Deming and Teller, usually referred to as the BDDT classification [Brunauer, 1940].

Reversible Type I isotherms are given by microporous solids presenting relatively small external surface areas, as is the case for some activated carbons, molecular sieve zeolites and certain porous oxides. They are concave to the p/p_0 axis and characterized by a limiting value of the amount adsorbed, which begins to set at relatively low relative pressure and is extended to the saturation pressure. Type I(a) isotherms are given by microporous materials having mainly narrow micropores, while Type I(b) isotherms are characteristics of materials with wider pore size distributions.

Reversible Type II isotherms are characteristics of the adsorption of most gases on non-porous or macroporous adsorbents, with unrestricted monolayer-multilayer adsorption. These isotherms are concave relative to the x-axis up to a certain point, normally referred to as Point B, when the middle almost linear section starts; Point B usually corresponds to the completion of monolayer coverage.

The Type III isotherms are convex in relation to the axis of the abscissas and do not present a Point B, with no monolayer formation. This indicates that the adsorbent-adsorbate interactions are relatively weak and the adsorbed molecules are clustered around the most favorable sites on the surface of a non-porous or macroporous solid. Type IV isotherms are characteristic of mesoporous adsorbents, as many oxide gels, industrial adsorbents and mesoporous molecular sieves. The adsorbent-adsorptive interactions and the interactions between the molecules in the condensed state rule the adsorption behavior in mesopores.

In Type IV(a) isotherms, capillary condensation is accompanied by hysteresis that occurs when pore widths exceeds a critical width, depending on the adsorption system and temperature. Completely

reversible Type IV(b) are observed for adsorbents having mesopores of smaller width. Type V isotherms are, to a certain pressure value, similar to the isotherms of Type III, which is an indication of relatively weak adsorbent-adsorbate interactions. Reversible stepped Type VI isotherms are associated with layer-by-layer adsorption on highly homogenous non-porous surfaces.

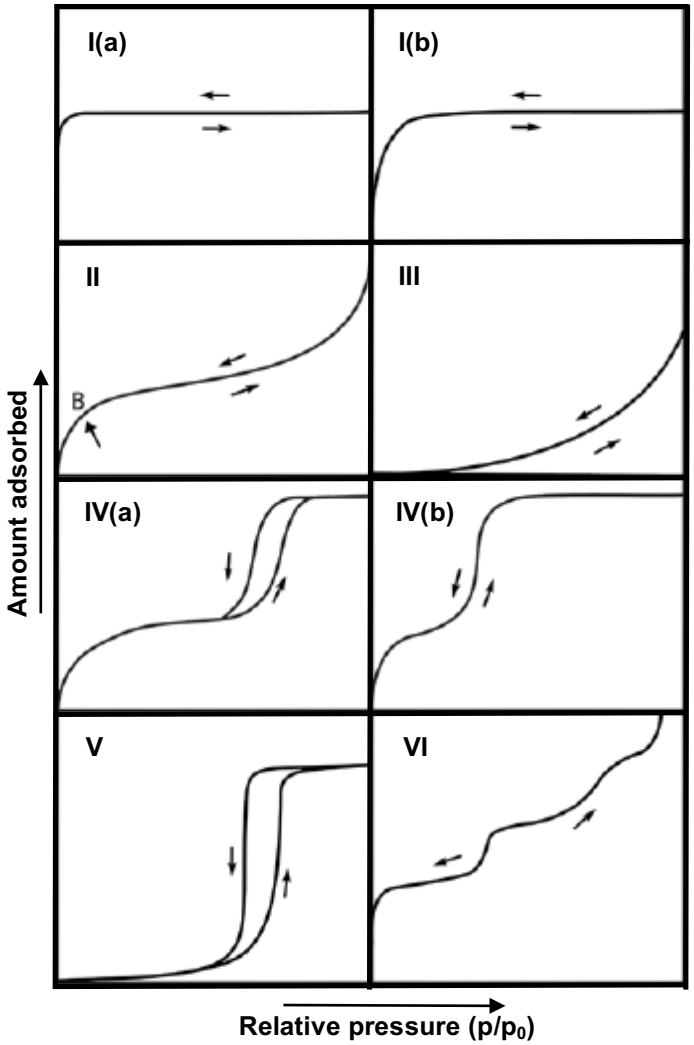

Figure 3.1- IUPAC classification of adsorption isotherms. *Adapted from* [Thommes, 2015]

3.2.3. BET equation

The work of Brunauer and Emmett, preceding the publication of the Brunauer-Emmett-Teller (BET) theory in 1938, reported that the adsorption isotherms of a number of gases, measured at temperatures at/or near their respective boiling points, were all S-shaped with certain distinctive features [Rouquerol, 2014]. Other authors, including Langmuir, recognized that this type of adsorption was not always restricted to monolayer coverage and an empirical approach was adopted by Emmett and Brunauer to ascertain the stage at which the multilayer adsorption began. They eventually decided that completion of the monolayer was characterized by the beginning of the nearly linear section of the adsorption isotherm (designated Point B). The surface area was then evaluated from the

amount adsorbed at Point B by making the further assumption that the completed monolayer was in a close-packed state.

A dynamic equilibrium of adsorption and desorption is recognized, but the possibility of forming adsorbed multilayers is included. BET model is based on the several assumptions: i) in each layer, the adsorption rate is equal to the desorption rate; ii) the heat of adsorption from the second layer is constant and equal to the vapor condensation heat; iii) when p is equal to p_0, the vapor condenses as a liquid and the ordinary number of adsorbed layers is infinite. The BET equation is expressed as:

$$n(p) = \frac{n_m \, C_{BET} \, p}{(p - p_0)\,[1 + (C_{BET} - 1)\,(p/p_0)]} \qquad \text{Equation 3.2}$$

where n(p) is the amount of adsorbed gas at pressure p, n_m is the adsorbed amount needed to fill the monolayer, p_0 corresponds to the vapor saturation pressure and C_{BET} is designated as the BET constant which is related to the adsorbate-adsorbent interactions.

The application of this equation in the experiment data allows the determination of the number of adsorbed moles in the monolayer (n_m) and the equivalent surface area (S_{BET}). BET equation can be linearized in different forms; in this thesis, the one proposed by Parra et al. in 1995 [Parra, 1995] is used:

$$\frac{1}{n\,(1 - x)} = \frac{1}{n_m} + \frac{1}{n_m \, C_{BET}} \left(\frac{1 - x}{x}\right) \qquad \text{Equation 3.3}$$

where x is the relative pressure (= p/p_0).

BET theory appeared to provide a sound basis for the identification of Point B as the stage of monolayer completion and the onset of multilayer adsorption. Since then, it has become a standard procedure for the determination of the surface area of a wide range of porous materials [Rouquerol, 2014]. On the other hand, it is now generally recognized that the theory is based on an oversimplified model of multilayer adsorption and that the reliability of the BET method is questionable unless certain conditions are prescribed.

The BET method can be applied to many Type II and Type IV isotherms, but needs to be applied with extreme caution for microporous materials (i.e. Type I isotherms and combinations of Types I and II or Types I and IV isotherms). In these cases, it may be very difficult to detect the formation of the monolayer from the multilayer adsorption and micropore filling, for which the linear range of the BET plot may be difficult to locate. The IUPAC has addressed this concern in the latest review in 2015 [Thommes, 2015], recommending a procedure to overcome this difficulty and to avoid any subjectivity in evaluating the BET monolayer capacity. The procedure is based on various criteria: i) the C_{BET} constant should be positive (i.e. a negative intercept on the ordinate of the BET plot indicates that the selected range of relative pressures for the application of the equation is not the appropriate one); ii)

the application of the BET equation should be restricted to the range where the term $n(1 - p/p_0)$ continuously increases with p/p_0; iii) the p/p_0 value corresponding to n_m should be within the selected BET range.

The mathematical approach proposed by Parra et al. in equation 3.3 does not only allow an easy determination of the right range of relative pressures for the correct application of the equation, but it also complies with all those criteria recommended by the IUPAC. Still, it should be reminded that the BET surface area values obtained from Type I isotherms represent apparent surface area, and should not be considered as realistic values.

3.2.4. Dubinin-Radushkevich equation (DR)

Dubinin introduced the concept of micropore filling, based on the early potential theory of Polanyi, in which physisorption isotherm data were expressed in the form of a 'characteristic curve' for a given adsorbent independent of temperature. The theory admits that the adsorption process involves the filling of the micropore volume and not the formation of several layers on the pore walls, as proposed by the BET, Langmuir or Polanyi models [Rouquerol, 2014].

If two vapors fill the same available micropore volume, it is assumed that the ratio of their adsorption potentials, $\beta=E/E_0$, is constant for the given adsorbent. The scaling factor β was termed the 'affinity coefficient', with E_0 taken as the reference value. In 1947, Dubinin and Radushkevich put forward an equation for the characteristic curve in terms of the fractional filling, of the micropore volume. The equation, based on the assumption that the micropore size distribution is Gaussian and the bulk liquid density at the operational temperature, is as follows:

$$\ln W = \ln W_0 - \left(\frac{R\,T}{\beta\,E_0}\right)^2 \ln^2\left(\frac{p_0}{p}\right) \qquad \text{Equation 3.4}$$

where W (cm^3/g) is the volume occupied by adsorbed phase at temperature T, W_0 (cm^3/g) corresponds to total volume of micropores, β is the affinity factor of adsorbate-adsorbent − which is 0.34 for nitrogen and 0.36 for carbon dioxide [Guillot, 2001]−, and E_0 (kJ/mol) is the adsorption energy.

The calculation of the micropore volume then consists on representing the amount of gas adsorbed form the equilibrium isotherm [ln W] vs the relative pressure [$\ln^2\left(\frac{p_0}{p}\right)$], and the volume of micropores [$\ln W_0$] is retrieved from the intercept of the representation in the linear region.

Besides the micropore volume, the total pore volume has been calculated from the equilibrium adsorption isotherm as the volume of gas adsorbed at a relative pressure of 0.99, expressed in terms of cm^3/g. The adsorbed phase is assumed to behave as a liquid phase, thus the amount of gas adsorbed in STP conditions from the isotherm is converted to liquid phase using the density of liquid gas, that in the case of N_2 at -196 ºC is 0.81 g/ml. Thus:

$$V_{PORES}\ (cm3/g) = V\ \text{gas adsorbed}\ (cm3/g, STP) \times 0.00154643 \qquad \text{Equation 3.5}$$

3.3. Physicochemical and structural characterisation

3.3.1. Elemental analysis

Elemental analysis was used for the chemical characterization of the carbon materials, more specifically for the quantification of carbon, hydrogen, nitrogen, oxygen and sulfur content, which provides useful information about the type of functionalities that might exist on the material's surface. For the determination of the carbon, hydrogen, nitrogen and sulfur contents the samples are typically combusted at high temperature (ca. 1200 °C) in a stream of oxygen, and the gases of combustion (CO_2, N_2, H_2O and SO_2) are measured in a single analysis (typically using infrared spectroscopy). For the analysis of oxygen, the sample is heated up to 1350 °C in inert atmosphere; the liberated oxygen is evolved in various forms (CO, CO_2, H_2O) and the gas is passed through a bed of graphite powder to reduce them to CO, then, CO is oxidized to CO_2 in a CuO catalysts and it is detected by infrared detector.

The determination of carbon, hydrogen and nitrogen was carried out by a LECO CHNS-932 (ASTM D-5373). Sulphur was measured in a LECO S-144DR (ASTM D-4239) analyzer, while oxygen was directly measured in a LECO VTF-900 CHNS-932 microanalyzer. For comparative purposes and to eliminate the moisture, all the samples were previously dried under vacuum at 120 °C for 17 h.

3.3.2. Point of zero charge (PZC)

The pH of the point of zero charge (PZC) of a given material is defined as a pH at which the net surface electrical charge (average of positive and negative charges) is zero. When the pH is lower than the PZC value the surface of the material is positively charged (attracting anions). When pH is above PZC the surface is negatively charged (attracting cations). By knowing the pH of the PZC of a material it is possible to predict its distribution of surface charges (i.e. if it will be positively or negatively charged) as a function of the environment; for instance, in an aqueous medium.

The PZC of the studied materials in this thesis was determined by a mass titration method. The experimental procedure consists in the dispersion of a fix amount of material in a suitable volume of distilled water; the suspension is continuously stirring under a nitrogen atmosphere at room temperature until equilibrium is attained (ca. 48 h) [Ania, 2007]. After equilibration, the pH value is measured using a glass electrode; then distilled water is added to the suspension in order to obtain a new dispersion with lower solids concentration. Typical dispersions of the materials in water employed were 2, 4, 6, 8, 10, 12, 14, 16 and 18 % (wt./wt.). The representation of the equilibrium pH versus solid weight percentage is a curve showing a plateau at high solids concentrations, which is taken as the PZC value of the material (typically between 8-12%).

3.3.3. UV-Vis diffuse reflectance spectroscopy (DRS)

Ultraviolet-visible (UV-Vis) spectroscopy is a useful technique for obtaining information about the electronic structure of the materials and their optical properties. It is based on the electronic absorption

of electromagnetic radiation when it interacts with matter in the range of wavelengths of ultraviolet and visible (190-800 nm). In the case of solid materials, the most used technique is the diffuse reflectance, observing the transition of electrons from the valence band to the conduction band and therefore allowing the calculation of the band gap energy, E_g.

Diffuse reflectance measurement is defined as the fraction of incident radiation that is reflected in all directions by the sample, due to absorption and dispersion processes. Predominates when the material of the reflecting surface is weak absorbent at the incident wavelength and when the penetration of the radiation is large in relation to the wavelength. Reflection has two components, specular and diffuse, with the latter providing useful information about the sample. The calculation of the diffuse reflectance can be rationalized by the Kubelka-Munk theory [Kubelka, 1931; López, 2012], which provides a relationship for the reflected radiation based on the absorption (k_{ab}) and dispersion (k_s) constant, according to:

$$F(R) = \frac{(1-R)^2}{2R} = \frac{k_{ab}}{k_s} \qquad \text{Equation 3.6}$$

where R is, the relative reflectance using a reference pattern.

In this work, for the calculation of the E_g a modified Kubelka-Munk function was used:

$$[F(R) x\ h\nu] \sim B\left(h\nu - E_g\right)^n \qquad \text{Equation 3.7}$$

where n is, a coefficient associated with an electronic transition (n=2 for an indirect allowed transition; n=3 for an indirect forbidden transition; n=1/2 for a direct allowed transition and n=3/2 for a direct forbidden transition) and B is the absorption constant. By plotting this equation ($[F(R) \times h\nu]^{1/n}$ versus $h\nu$), that corresponds to Tauc representation [Tauc, 1966], E_g value was obtained by extrapolating the slope to $[F(R) \times h\nu]^{1/n} = 0$.

UV-Vis absorption spectra were recorded on a Shimadzu spectrometer equipped with an integrating sphere using $BaSO_4$ as a blank reference.

3.3.4. X-Ray diffraction spectroscopy (XRD)

The X-Ray diffraction spectroscopy is the most widely used method to identify crystalline structures as it allows a rapid and non-destructive analysis of multi-component mixtures without the need for extensive sample preparation. X-Ray is an electromagnetic radiation of the same kind of visible light, strongly energetic due to its short wavelength (10^{-2} to 10 nm). Generally, the longer wavelength used for inorganic and organic materials studies vary between 0.05 and 0.25 nm due to the interatomic distances of the materials located in this interval. The diffractograms are characteristic of each crystal and result from the interference between the waves associated with X-Ray and the electronic cloud of the constituents of the crystal lattice. Diffractograms correspond to the representation of the diffracted intensity as a function of the incident angle (typically 2θ). Their analysis enables to determine the distribution of atoms, ions or molecules in a crystal lattice.

X-Ray phenomenon is described by Bragg law equation 3.8 that predicts the direction in which constructive interferences occur between beams coherently scattered X-rays by a crystal:

$$n\lambda = 2d\,\sin\theta \qquad \text{Equation 3.8}$$

where λ is the wavelength of the incident radiation, d is the interatomic distance and θ corresponds to the diffracted angle. Furthermore, other applications are found in the quantitative analysis of crystalline compounds, the determination of many parameters like coefficient of thermal expansion, determination of the crystal symmetry, as well as the determination of the crystallite size [Warren, 1965]. In this work, the diffractograms were obtained in a Bruker D8 Advance instrument operating at 40 kV and 40 mA, using Cu Kα (λ= 1.5406 nm) radiation.

3.3.5. Scanning electron microscopy (SEM)

Scanning electron microscopy technique allows the observation and characterization of the external surface of the materials giving information about the morphology of microscopic zones. In this technique, the incident electrons interact with atoms in the sample surface producing various signals that can be detected and provide an image that displays information about the topography and composition of the material surface.

Scanning electron microscopy images were obtained from a FEI QUANTA FEG 650 model coupled to an EDX (Energy Dispersion X-Ray) detector.

3.4. Photocatalytic degradation reactions

Photodegradation experiments in the presence and absence of a catalyst (photolysis) were performed under the same experimental conditions and at room temperature. The experimental set-up has been described elsewhere [Velasco, 2012b]. Briefly, a catalyst loading of 1 g/L was dispersed in ca. 500 mL of synthetic or real wastewater in a glass photorreactor. The UV irradiation source was provided by a high-pressure mercury lamp (Helios ItalQuartz, 125 W), vertically suspended in a cylindrical, double-walled pyrex jacket cooled by flowing water, immersed in the solution. The water cell was used to control the temperature during the experiments, preventing any overheating of the suspension due to the irradiation and also avoiding photothermic effects due to irradiation. A high-pressure Hg lamp (125 W) was used as irradiation source, emitting between 200-600 nm. However a pyrex jacket was used to filter-out the irradiation below 360 nm. The corresponding spectrum of the lamp with the filter is shown in Figure 3.2.

At regular intervals of 1, 3 and 6 hours, aliquots of the solution were extracted and analyzed. The samples were previously filtered using regenerated cellulose filter having mean pore size of 0.45μm. The aliquots were analyzed by reverse-phase HPLC (Spherisorb C18 column 125 mm x 4 mm, using methanol-water mixture as mobile phase, using a photodiode array detector) to measure the evolution of phenol and its photooxidation intermediates upon irradiation. The photodegradation of all samples was always performed two times for posterior analysis.

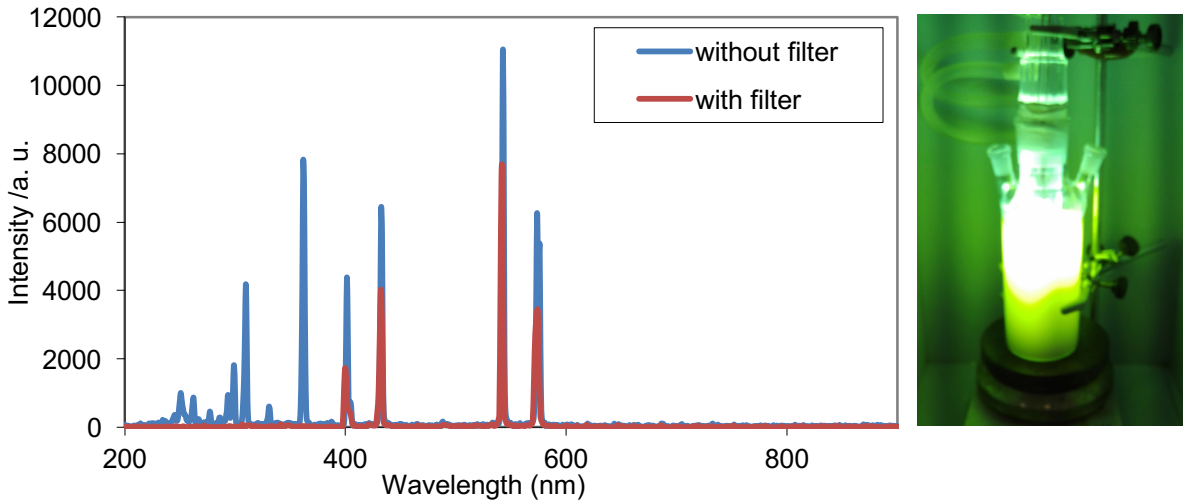

Figure 3.2 - Emission spectrum of a high-pressure mercury lamp (in the right) . Irradiation below 360 nm was cut-off with a pyrex filter

3.5. Ecotoxicity measurements

The ecotoxicity was evaluated by means of the *Vibrio fischeri* luminescence inhibition test, using a Microtox apparatus Figure 3.3. The test in based on the luminescence decay of the bacterium when it is exposed to a chemical agent, provided that the signal is proportional to the bacterial population. The concentration of the pollutant that causes a 50% reduction in light after exposure is designated as the EC_{50}. The protocol used was adapted from the recommended test provided by the supplier of the apparatus, and consisted on suspending the bacteria on a solution of the pollutant in the present of an inert electrolyte (ca. NaCl) at room temperature and measure the decrease in the bacterial luminescence after a certain time of exposure.

Figure 3.3 – *Microtox - Model 500 ANALIZER from [Microbics Corporation, 2010]*

All the solutions were prepared in the laboratory, assuring conservation and preparation indications, with the exception of the Microtox reagent.

Ultra-high purity water (Milli-Q quality) was used to prepare the solutions, as well as sterilized glass vials (> 100° C). The blanks were prepared with pure water, 2 wt.% and 22 wt.% NaCl solution. All solutions were sealed and stored in the refrigerator at 4°C. The reagents needed for the ecotoxicity test are:

- Reconstitution solution: high purity water;

- Diluent: 2% sodium chloride solution;
- Osmotic adjusting solution (OAS): 22 wwt. % sodium chloride solution;
- Microtox reagent: a lyophilized culture of *Vibrio fischeri.*

The experimental protocol consists on various steps:

a) Sample pre-treatment: for pH adjustment between 6-8 units, using 1M HCl and 0.01M NaOH (Crison pHmeter).

b) Bacteria reconstitution. The bacteria reagent stored in a freezer (-20ºC) was transferred to a refrigerator (4ºC) for 20-30 minutes (to avoid a thermal shock). Afterward, ca. 1000 µL of reconstitution solution (previously stabilized at the analysis temperature in a cuvette for 10-15 min) were rapidly added to the bacteria vial (by inverting the cuvette), mixed by swirling for a few seconds and transferred to the precooling well of the apparatus. It is important to mix the reagent repeatedly (aspirating and dispensing ca. 500 µL of the solution about 5-10 times) to guarantee a good dispersion. The rehydrated reagent is allowed to stabilize for about 15 minutes before its use.

c) Sample preparation with the osmotic adjustment (OAS). About 2500µL of test sample were placed in a cuvette in well A5, and 250µL of OAS were added and carefully mixed with the micropipette (aspirating and dispensing the solution 3-5 times). Then, 750µL of well A5 were discarded. After that, 1000 µL of diluent were transferred to A1, A2, A3 and A4 cuvettes, so as to make a full series 1:1 serial dilution with the sequence as indicated below (it should be noted cuvette A1 is used as control (since no sample is added to this well):

- Transfer 1000µL from A5 to A4 (mixing by aspirating and dispensing the solution 3-5 times with the same micropipette);
- Transfer 1000 µL from A4 to A3 (mixing as indicated above);
- Transfer 1000 µL from A3 to A2 (mixing as indicated above);
- Discard 1000 µL from A2 in order to maintain a constant volume in all the cuvettes;
- Allow 15 minutes for 15ºC temperature equilibration.

d) Pipetting 500µL of diluent into cuvettes B1, B2, B3, B4 and B5 along with 10µL of reconstituted bacterial reagent (from the precooling well), allow to rest for 15 minutes at 15^{o}C, and start the reading. For starting the reading process, cuvettes B1 to B5 are placed into the read position (well) of the equipment; then the CALIBRATE button is pressed to set the digital reading, followed by pressing START in the computer. This allows to obtain the initial light (I0) levels for each cuvette. Immediately, and without removing the cuvettes of the A series from the incubator wells, ca. 500µL of cuvettes A are transferred to cuvettes B (ca. A1 to B1, A2 to B2, and so on), and allowed to rest for a given exposure time, TEXP (i.e., 5 and 15 minutes in this work) after the first sequence. Then the cuvettes are cycled again to the read position in the same order to record the intensity I_{TEXP} (i.e., I_5 and I_{15} in this work). All the tests were done within the first 3 hours of reconstitution of the bacteria, and contrasted with the reference chemicals recommended by the supplier (i.e., $ZnSO_4$ and phenol) in

order to confirm the sensitivity of the bacteria and at least three repetitions were assured for every test perform during this thesis.

3.5.1. Ecotoxicity data treatment

The presented calculus was achieved by consulting several documents on the literature.

Blank ratio Once the bioluminescence signals were record, a few parameters were calculated in order to better interpret the data.

Blank ratio, BR(t): defined as the ratio between blank readings at different times. This value is used for normalization of the sample's reading. The reason for this normalization is to overcome the differences in the light intensity of different blanks due to external factors, ensuring a correction for the remaining readings, and allows to calculate a correct gamma(t). Typically, blank ratio values should range between 0.6 and 1.3.

$$BR(t) = \frac{I(t)}{I(0)} \qquad \text{Equation 3.10}$$

I(t) is the final time light intensity reading of a sample and the I(0) is zero time light intensity reading of a sample.

Corrected light intensity, Icorr(t): defined as the value of reading for time t, I(t) after the blank ration correction according to:

$$Icorr(t) = I(0) * BR(t) \qquad \text{Equation 3.11}$$

Gamma, γ: defined as the ratio of activity lost to activity remaining per reading at a given time by Johnson et al. (1974) , computed by the formula:

$$\gamma(t,T) = \frac{corrected\ light\ lost}{light\ remaining} = \frac{Icorr(t) - I(t)}{I(t)} \qquad \text{Equation 3.12}$$

where Icorr(t) is the light emission of the test bacteria that is lost corrected by the blank ratio, and I(t) is the final emission produced after the exposure time T.

Gamma should be a positive value; otherwise the bacteria's light emission is not stable (blank reading) or decreasing (with contamination), but in fact is growing.

Relation between log (γ) vs log(C): $\log(\gamma) = b(\log C) + \log a$, where C is the concentration of pollutant. The fitting of the curve allows to calculate the values of EC_X, defined as the concentration of pollutant needed to cause a fall of X % in the bioluminescence signal. Typically, values of EC_{50} are reported, calculated as the concentration when γ=1, and EC20 when γ=0.25.

Percentage of normalized light loss, vs the initial light of the blanks, calculated as follows:

$$Normalizes\ \%\ light\ lost = \frac{BR(I0) - I(t)}{BR * I(0)} * 100 \qquad \text{Equation 3.1}$$

Chapter

4. Results and Discussion

4.1. Characterization

The main goal of this master thesis was to evaluate the impact of the incorporation of nanoporous carbons (either as photocatalysts or additives to semiconductors) on the ecotoxicological properties of the treated water after the photocatalytic treatment, using phenol as a model organic pollutant commonly present in industrial wastewaters. To attain this goal, commercially available titanium dioxide powders were selected as semiconductor, and an activated carbon (coal–based) as additive. The nanoporous carbon was selected based on its photochemical activity demonstrated towards the photooxidation of phenol from aqueous solution under UV-Visible light.

The selected photocatalysts were characterized in terms of porosity, structure and composition using a varied of complementary techniques such as gas adsorption, X-rays diffraction or diffuse reflectance. The textural characterization of the catalysts was carried by means of the N_2 adsorption isotherms at -196 ºC, shown in Figure 4.1. The main textural parameters obtained from the gas adsorption data are compiled in Table 4.1.

4.1.1. Adsorption of gases

The nanoporous texture of the materials -TiO_2, CQ and TiO_2/CQ- was characterized by gas adsorption. Figure 4.1 presents the measured gas adsorption isotherms of nitrogen at -196ºC for the materials tested.

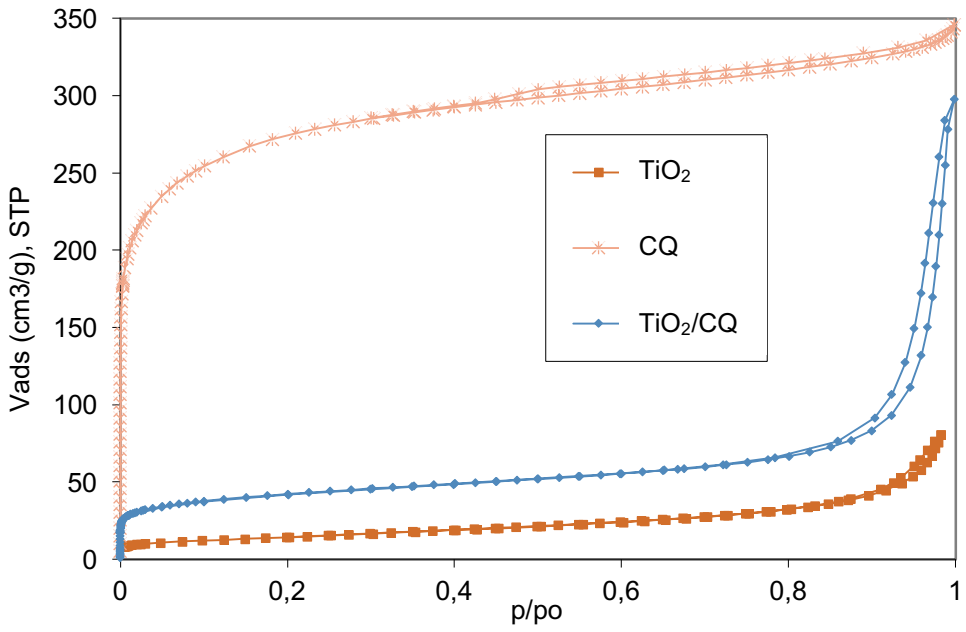

Figure 4.1 – Nitrogen adsorption/desorption isotherms at -196ºC of the studied photocatalysts.

As seen, TiO_2 (P25) is a non-porous material which displays a type II isotherm according to IUPAC classification [Thommes, 2015] and a low total pore volume. The hysteresis loop appearing at high relative pressures is associated to interparticle condensation in the particles of the semiconductor of

nanometric dimensions, rather than to mesoporosity. This was further confirmed by the SEM images of the semiconductor (Figure 4.2). On the other hand, the nanoporous carbon showed a type I isotherm, which is characteristic of a highly microporous material. The TiO_2/carbon composite showed a mixed type I/IV shape, indicating that it inherited the textural properties of both components in the mixture. The hysteresis loop of the TiO_2/carbon composite is more pronounced than in TiO_2, and is also due to interparticle condensation, since the preparation of the hybrid TiO_2/carbon photocatalyst was done by physical mixture of both components (thus the creation of new intraparticle porosity of mesoporous dimensions is not expected).

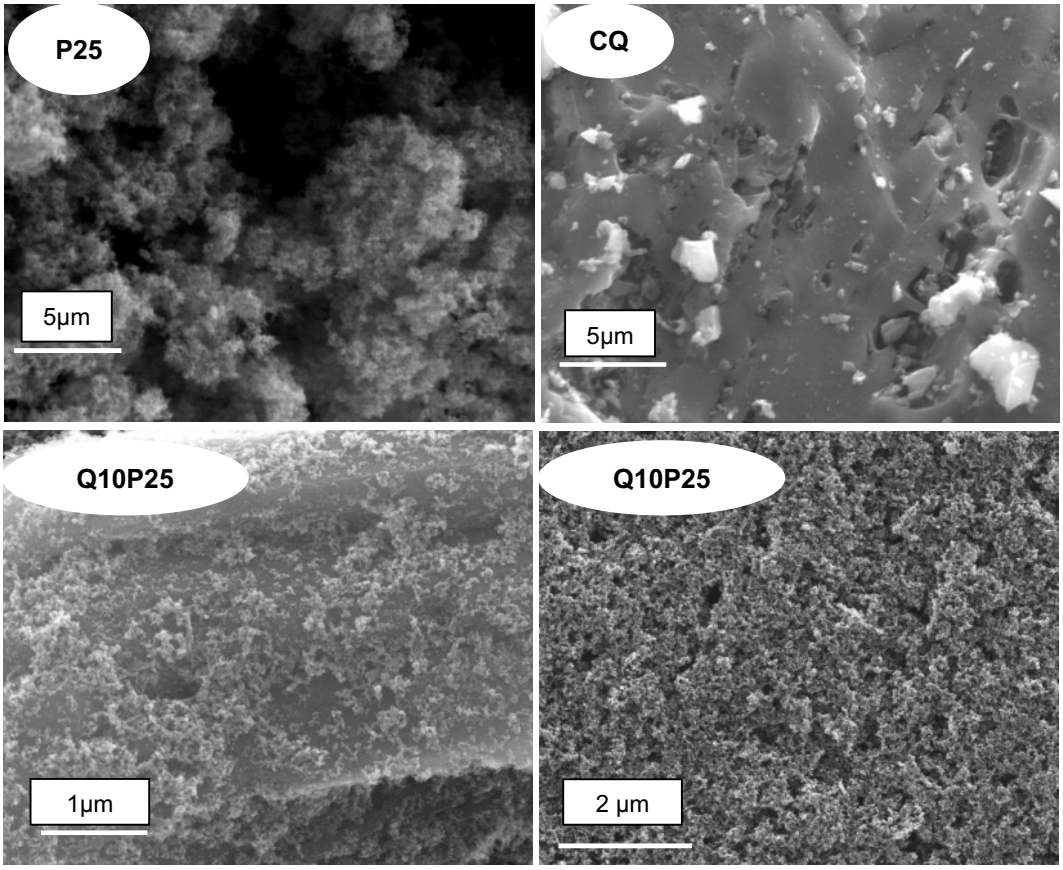

Figure 4.2 - SEM micrographs of the studied photocatalysts.

Table 4.1 - Main textural parameters of the studied photocatalysts obtained from the analysis of the N_2 adsorption data

	S_{BET}	V_{TOTAL}*	$V_{MICROPORES}$**
	[m^2 g^{-1}]	*[cm^3 g^{-1}]*	*[cm^3 g^{-1}]*
P25	52	0.088	0.019
Ti90:Q10	151	0.443	0.052
CQ	1025	0.530	0.406
** evaluated at relative pressure of 0.99*			
*** evaluated by the Dubinin-Radushkevich method*			

The surface area and pore volume of the TiO_2/carbon composite was slightly higher that of the bare semiconductor, as expected based on the theoretical value calculated considering the loading of titania and the nanoporous carbon in the composite. The good agreement between the experimental and theoretical values for surface area and pore volumes suggests an homogenous dispersion of the carbon and TiO_2 matrices in the composite. Similar observations have been reported for activated carbon-titania composites with loadings between 5-50 % prepared using a similar procedure [Haro, 2012].

The XRD patterns of the catalysts are shown in Figure 4.3. The patterns corresponding to TIO_2 showed peaks associated to the anatase (25.3º) and rutile (27.4º) crystalline phases of TiO_2, which are both present in the solid (although anatase is the dominant phase). In the case of the nanoporous carbon, the patterns show ill-defined and broad peaks at 25º and 44º, corresponding to the reflections (002) and (100) associated to the presence of graphitic structures. The peaks at 21º and 27º are characteristic of silica (quartz phase) and are associated to the ashes of activated carbon, as confirmed by chemical analysis (Table 4.2). The C/TiO_2 composite showed XRD patterns similar to those of the two precursors, although with slightly lower intensities, indicating that the crystalline phases of the inorganic oxide and carbon are not modified.

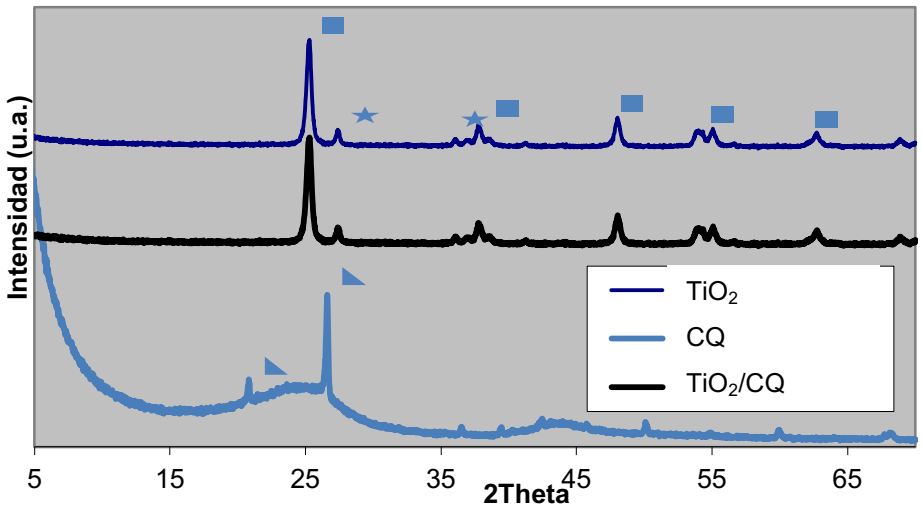

Figure 4.3 - X-ray diffraction patterns of the P25, carbon Q and composites studied. Peak marking correspond to: ■ anatase; ★ rutile; ◣ SiO_2

Table 4.2 - Chemical analysis (wt.%) of the nanoporous carbon on a dry basis.

	Carbon	Hydrogen	Oxygen	Nitrogen	Ashes
	[wt.%]	[wt.%]	[wt.%]	[wt.%]	[wt.%]
CQ	86.79	0.54	1.89	0.63	10.15

An important property of materials used in photocatalytic applications is their optical band gap, which can be estimated using UV-visible Diffuse Reflectance (UVDR) spectroscopy. The UVDR spectra of the catalysts are shown in Figure 4.4. The spectrum of P25 clearly shows the characteristic absorption edge of anatase-form TiO_2 (predominant in P25) with the highest absorption in the UV region. The corresponding energy band gap evaluated for P25 was 3.16 eV, which is in good agreement with the values reported in the literature for this compound [Grzechulska, 2003; Nagaveni, 2004].

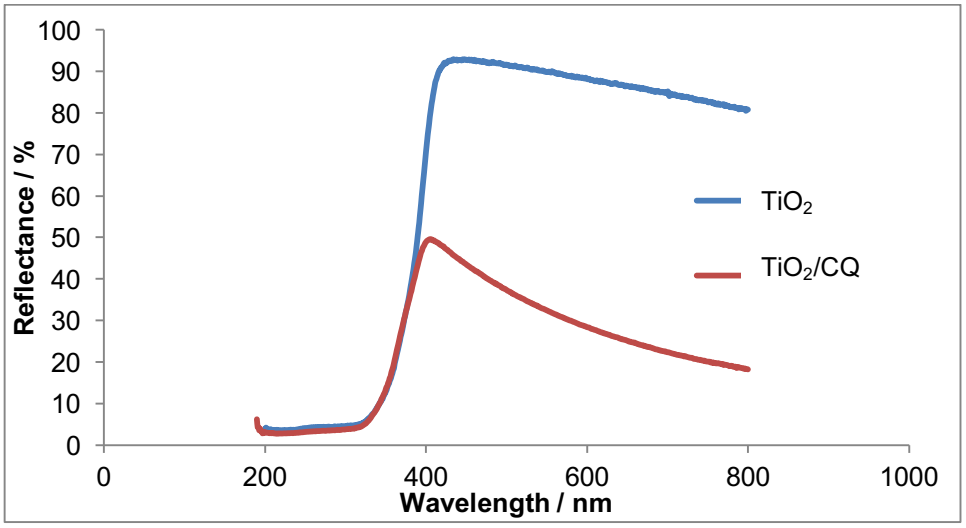

Figure 4.4 - **U**V-visible Diffuse Reflectance patterns of the studied photocatalysts.

For the TiO_2/carbon composite, the absorption of light in the visible region is pronounced as evidence in the drop of reflectance intensity in the pattern. Since the amount of carbon in the composite is not very high, the absorption edge in the UV region due to TiO_2 is still clearly observed, and overlaps with that of the TiO_2, as expected based on the method of preparation of the hybrid composite. This confirms that the optical band gap of the TiO_2/carbon composite is similar to that of bare TiO_2, thus any modification of the photocatalytic yield cannot be attributed to differences in the optical band gap, but rather to other effects associated to the carbon matrix itself such as: intrinsic photochemical activity of the carbon matrix giving rise to the photogeneration of radical species, the photoelectron withdrawal effect in the electron density of the carbon matrix (reducing recombination phenomena of hole/electron pairs), the porosity inherited from the carbon material, among most representative. This contrasts with previous works reported in the literature for composites with other carbon materials and loadings, where the optical response of the semiconductor is modified by the incorporation of the carbon additive, although differences are linked to the synthetic methods [Leary, 2011].

Additionally, the surface pH of the point of zero charge of the photocatalysts rendered values of 3.7, 9.1 and 6.2 for TiO_2, carbon Q and TiO_2/carbon composite, respectively. This parameter indicates the acidic nature of the semiconductor and the hybrid composite, as opposed to the basic character of the nanoporous carbon.

4.2. Optimization of the experimental protocol

The determination of the EC_{50} value of a given pollutant depends strongly on various experimental parameters, such as the solution pH, the time of exposure, the nature of the sample, the electrolyte concentration and so forth. In order to validate the results obtained in this master thesis with those reported in the literature, the first objective was to optimize the experimental protocol for the determination of the EC_{50} value. Phenol and zinc sulfate are most common reference compounds for the determination of EC_{50} values based on bioluminescence tests of *Vibrio fischeri*. In this master thesis, phenol was selected over zinc sulfate, since it is a toxic compound frequently found on wastewaters from factories, and its ecotoxicity has been widely investigated in the literature, which allows the comparison of our data with that of other authors (and validation of the method).

The parameters to be optimized were the solution pH, the aging of the sample during the measurements, the time of exposure, the electrolyte concentration and the pollutant concentration. It should also be mentioned that all the EC_{50} values were performed in at least triplicate, and presented values correspond to the average of 3 repetitions; additionally, the EC_{50} values were calculated by 5 different methods. A concentration of 100mg/L of phenol in water was selected as starring point for the optimization, based on our previous studies on photocatalytic degradation of synthetic phenolic solutions [Velasco, 2012b].

4.2.1. pH adjustment

Bacterium *Vibrio fischeri* can develop normally at pH values ranging from 4.5 to 9.5 [Lichtfouse, 2005]. According to literature, for an optimum sensitivity of the bioluminescence assays using these bacteria, the pH should be adjusted between 6 and 8 [Waters, 1985]. In this work, the pH of the samples was about 5.68, thus it was adjusted to ca. 6.97 with NaOH. Table 4.3 shows the values corresponding to EC_{50} obtained after 5 min of exposure for a solution of phenol with and without pH adjustment. As seen, the EC_{50}-t' slightly increased after the pH adjustment in NaOH (pH value of ca. 7), although the changes were quite subtle (ca. lower than 10 %). The only exception was the value obtained after 60 minutes of exposure (EC_{50} -60'), about 1.3 times lower than that without pH adjustment (ca. 20 % variation).

Table 4.3 – Effect of pH on the ecotoxicity expression (EC_{50} t') of an aqueous phenol solution at various exposures times -t- between 5 and 60 min.

EC_{50}- t [mg/L]	***no pH adjustment***	***pH adjusted in NaOH***
EC_{50} -5'	17	19
EC_{50} -15'	20	22
EC_{50} -30'	23	24
EC_{50} -60'	41	32

Based on our results, and considering the common practice in the literature, the pH adjustment between 6-8 units was selected in further experiments, allowing comparative studies with other laboratories.

4.2.2. Selection of time exposure

The time of exposure or incubation time is very important in the bioluminescence assays, since it may affect the population and viability of the bacteria. If times are without significance (either too short of too long), the study may be compromised, thus it is necessary to evaluate the confidence of the assays performed, concerning their reproducibility. Table 4.4 shows the data corresponding three different repetitions of EC_{50} values at different exposure times between 5 and 60 minutes for an aqueous phenol solution.

Table 4.4 – Effect of incubation time on the EC_{50} t' of phenol

EC_{50}- t [mg/L]	***Test 1***	***Test 2***	***Test 3***
*EC_{50} 5'**	16	17	19
*EC_{50} 15'**	19	19	22
*EC_{50} 30'**	21	20	24
*EC_{50} 60'**	23	24	32

** pH adjustment with NaOH between 6 and 8*

As seen, the variability of the data after 60 minutes was too large (ranging between 5 and 25 %) indicating instability of the signal after long periods of incubation; thus the 60-minute's incubation time was immediately excluded. Also, it should be noted that not many works in the literature report the EC_{50} value after 60 minutes of exposure, likely due to similar reasons related to the uncertainty of results. Between the 5 and 15 minutes, in the three tests, the variability of the EC_{50} values was much smaller (on average ca. 14-16 %). For further studies, exposure times of 5 and 15 minutes were selected, since both values are also frequently reported in the literature.

4.2.3. Aging of the solution

The aging of the pollutant's solution is typically considering one of the main factors affecting the measurement of EC_{50}-t' values, although scarce information is given on adequate sample storage protocols. To evaluate this issue, solutions were prepared and tested in the same day, and then re-measured after being stored between 2-8ºC in dark glass bottles for 72 h to prevent direct sunlight.

Data in Table 9 shows that, under these conditions, the solutions were quite stable and the values of EC_{50} at 5 and 15 minutes of exposure were also robust and reliable (differences lower than ca. 5 %).

Table 4.5 - Effect of aging of the sample on the EC_{50} t' of phenol

EC_{50}- t [mg/L]	***Same day***	***72 hours later***
EC_{50} 5'	16	16
EC_{50} 15'	20	19

The aging of the solution doesn't affect the EC_{50} t', but it needs to be kept in the ideal conditions such as: between 2-8ºC, in a dry area, out of direct sunlight and stored in a dark bottle.

4.2.4. Electrolyte concentration

The solution of the pollutant to be analysed by bioluminescence assays is often prepared using a diluent containing ca. 2 wt.% NaCl as inert electrolyte, although some works can be found recommending the use of distilled or deionized water. In the case of *Vibrio fischeri*, upper and lower limits of growth have been reported for NaCl concentrations ranging from 0.0% to 9.0% [Soto, 2009], given the fact that this is a marine bacteria. Indeed, most common experimental protocls recommend the use of 2 wt.% NaCl and OAS in 2 wt.% NaCl as diluent for this reason. In this work, we have explored the use of two solutions prepared with and without 2 wt.% NaCl as diluent. Data in Table 4.6 shows that the values obtained for 5 and 15 minutes of exposure were quite similar in the presence and absence of NaCl as inert electrolyte. Considering this, and since the aim of this study is to study the EC_{50} values of solutions with low concentrations of electrolyte, after photocatalytic degradation, further experiments were prepared in distilled, deionized water.

Table 4.6 - Effect of NaCl as diluent electrolyte on the EC_{50}-t' of phenol.

EC_{50}- t [mg/L]	***Deionized water***	***Diluent***
EC_{50} 5'	17	19
EC_{50} 15'	19	22

4.2.5. Optimized parameters for phenol

Considering all the above remarks, the optimized protocol for the determination of the EC_{50} values of 100 ppm of phenol in water, using the bioluminescence assays of *Vibrio fischeri* bacterium were: pH adjustment of water aliquots -with NaOH or HCl- between 6 and 8; time of incubation of 5 and 15 minutes; samples prepared or reconstituted in distilled, deionized water; measurements of fresh solutions or after 72 h of preparation (when possible).

With this protocol, the obtained values were: EC_{50} 5' ≃ [19 – 20] mg/L and EC_{50} 15' ≃ [21 – 23] mg/L.

4.3. Ecotoxicity of phenol degradation intermediates

In chapters 1.4 and 3.4 it was mentioned that the photodegradation of phenol originates mainly polyhydroxylated aromatic compounds as intermediates, mainly *p*-benzoquinone, hydroquinone, resorcinol and catechol. Thus exploring the ecotoxicity of phenol degradation implies to know the ecotoxicity of its degradation intermediates. For this reason, in this work we have also determined the EC_{50} values of dihydroxylated benzene in solution. This is most important, since there is plenty of uncertainty regarding the ecotoxicity of these compounds, with different laboratories reaching dissimilar results, and some of them not detailing the experimental protocol used for its determination.

The initial concentration of phenol intermediates for the bioluminescence tests was lower than that of phenol (ca. 100 ppm), since most of them showed much higher ecotoxicity values than phenol itself. Thus it was not possible to measure high concentrations of these pollutants and dilutions were needed. As an example, in the case of *p*-benzoquinone, an initial solution concentration of 0.26 ppm was prepared, and 4 dilutions were made in the experimental protocols in order to obtain meaningful luminescence values. At converse, in the case of resorcinol, the concentration needed to be increased up to ca. 1000ppm, pointing out to a much lower ecotoxicity than phenol and *p*-benzoquinone.

Figure 4.5 present the loss in the luminescence signal of different repetitions after 5 and 15 minutes of exposure for *p*-benzoquinone solutions ranging between 0.023 and 0.026 mg/L. First of all, it can be inferred that the reproducibility of the measurements is quite good, since the dispersion in the values is low; thus for further measurements only the average values are presented.

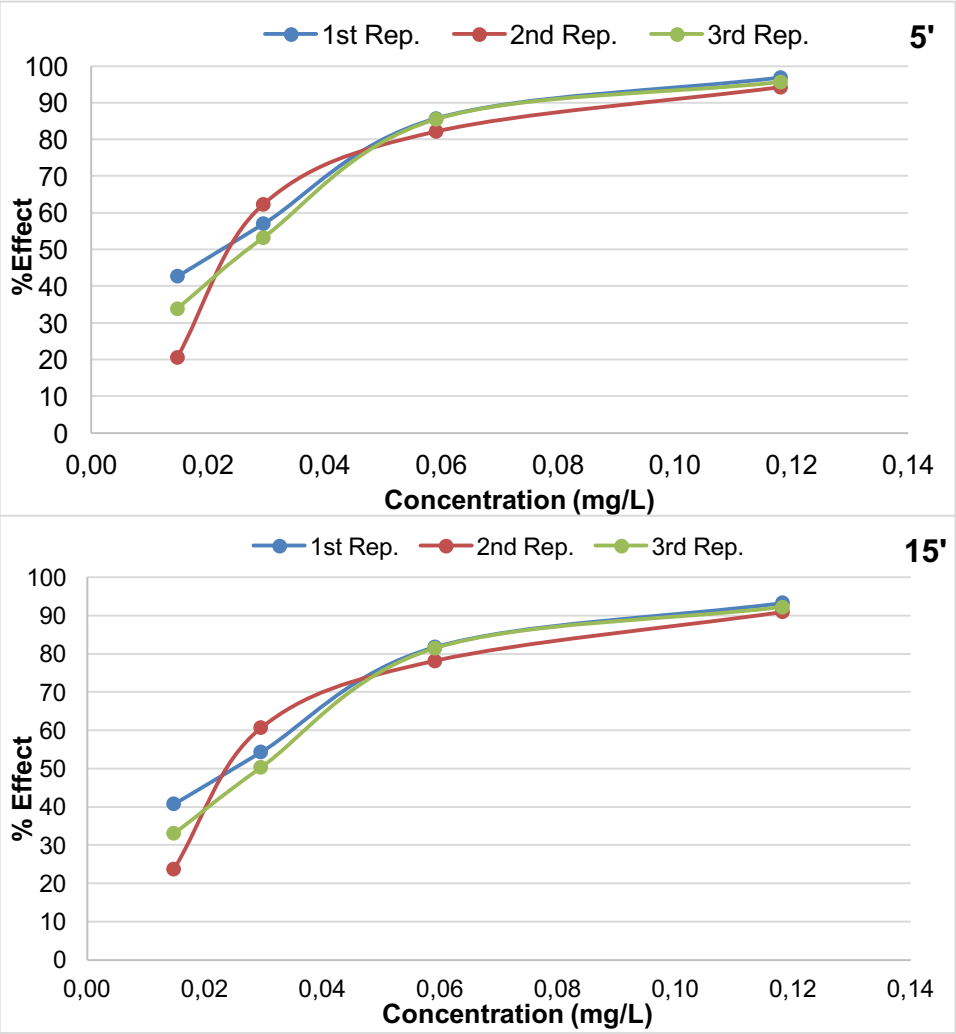

Figure 4.5 - EC_{50} 5' and EC_{50} 15' for *p*-benzoquinone 0.023-0.026 mg/L.

The EC_{50} 5' and 15' values for all the intermediates are presented in Table 4.7 (example of detailed calculations can be found in Annex A). As seen, the ecotoxicity values followed the trend: *p*-Benzoquinone > Hydroquinone >>>>> Catechol > Phenol >>> Resorcinol. Considering their different ecotoxicity values, it is expected that the ecotoxicity of the solution after the degradation treatment will be much affected by the mechanism of degradation, and hence the preferential formation of certain intermediates over others.

Table 4.7 – EC_{50} values of phenol aromatic intermediates

Intermediate (concentration of solution tested)	***$EC_{50\text{-}5`(mg/L)}$***	***$EC_{50\text{-}15`(mg/L}$***
Catechol (50ppm)	14-17	7-9
Hydroquinone (0.25 ppm)	0.035-0.046	0.038-0.049
Resorcinol (1000ppm)	159-231	129-150
p-Benzoquinone (0.26ppm)	0.023-0.026	0.024-0.026

4.4. Ecotoxicity measurements of synthetic solutions

For clarity purposes, Figure 4.6 explains the repetitions made for the ecotoxicity measurements, for both the synthetic solutions and real wastewater (with and without catalysts) to assure the accuracy of the data (in terms of repeatability and reproducibility).

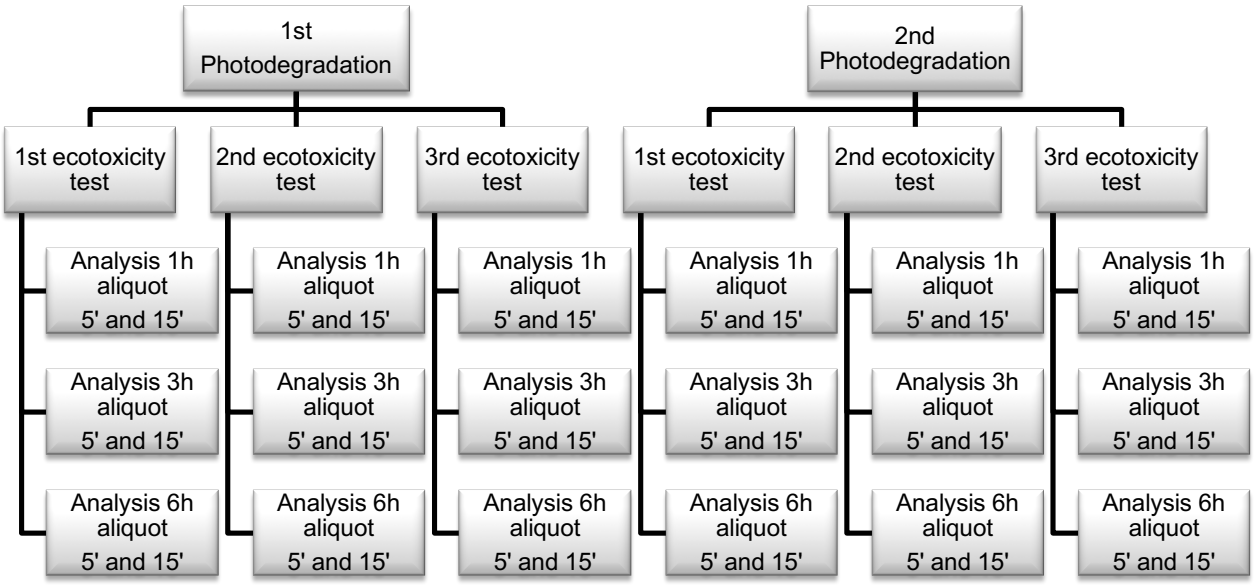

Figure 4.6 - Repetitions made for the ecotoxicity measurements for each catalyst

4.4.1. Synthetic solutions

4.4.1.1. Photolysis

Initially, the photodegradation tests were performed without a catalyst so as to evaluate the degradation of phenol exclusively due to the presence of the light (photolytic breakdown). For this purpose, a synthetic solution of phenol with an initial concentration of 100 ppm was irradiated as detailed in the experimental section for 6 hours. The ecotoxicity was measured for aliquots taken at fixed intervals (i.e., 1, 3 and 6 hours) during the photolysis.

Figure 4.7 show the trend of loss of bioluminescence signal (normalized vs the blank) with the dilution factor of the initial concentration of the solution after various irradiation time and after 5 and 15 min of incubation of the bacteria. The dilution factor is an indication of the concentration of the solution, in terms of volume; this allows to compare the data of solutions where the concentration of the pollutants varies over time (as it is the case in photocatalytic tests). Thus, 100 % refers to the pristine undiluted aliquot, whereas 20 % indicates that the same aliquot has been diluted with a factor of 0.2. At the same time, the loss of bioluminescence signal indicates the impact of the photooxidation process on the aliquots. Thus, the samples show a higher ecotoxicity when the impact in the luminescence signal is higher for low dilution factors.

The fall in bioluminescence showed a gradually growing trend with the relative concentration, reaching 50 % of inhibition at relative concentration of about 45 and 55 %, regardless the irradiation time (1, 3 and 6 hours) and for both incubation periods of 5 and 15 min. Data also show that the toxicity of the solution decreased from 1 to 3 hours or photolytic reaction; however, longer irradiation times resulted in an increase in the toxicity of the solution (ca. values were slightly higher after 6 hours than after 3 hours), indicating the gradual formation of more toxic compounds with the irradiation time.

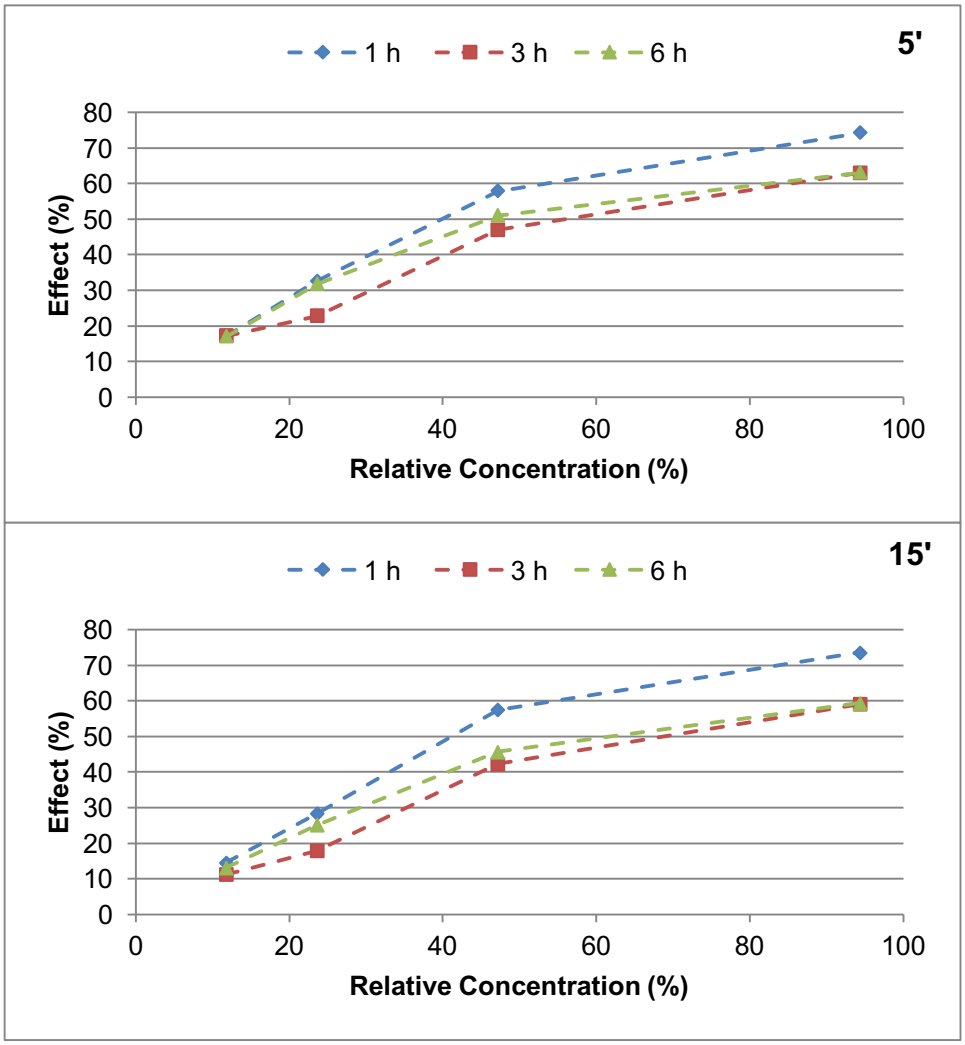

Figure 4.7 - Loss of bioluminescence signal after 5 and 15 min of incubation for the photolytic degradation of phenol at various irradiation times (ca. 1, 3 and 6 h).

This can be explained considering the formation of intermediates during the photodegradation reaction. As seen in

Figure 4.8, the direct degradation of phenol in the absence of a catalyst (photolytic reaction) was about 3 % in terms of phenol conversion after 6 hours, with no noticeable mineralization. This is due to the irradiation characteristics of the lamp, that was used with a pyrex filter to cut-off the light below 360 nm. The fraction of light absorbed by the aqueous phenol solution above 360 nm is negligible [Bayarri, 2007; Velasco, 2014], and the energy of the photons is not high enough to promote the oxidation of

phenol to a large extent. When photons of higher energy are used (UV light), the photolytic degradation of phenol can reach values of up to 85 % phenol conversion [Velasco, 2012b]. Despite the low amount of phenol degraded under these conditions, small amounts of intermediates were detected, demonstrating the photooxidation of phenol. Regarding this, catechol was found to be the dominant intermediate over quinones, with gradually increasing concentrations in all the cases. The occurrence of quinones, even at low concentrations, would be the reason of the increasing toxicity of the solution with the irradiation time. Indeed, the mineralization of the solution, as evaluated from the determination of the Total Organic Carbon Content was almost negligible for the photolytic reaction (ca. below 1 %).

In sum, the low removal efficiency of both phenol and its intermediates after 6 hours of irradiation make the photolytic breakdown a limited approach for the treatment of phenolic solutions.

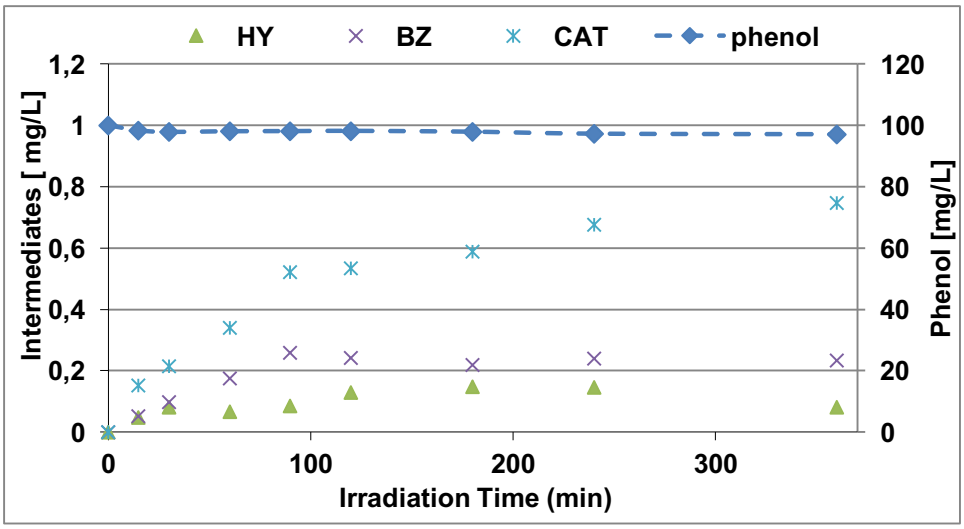

Figure 4.8 - Evolution of phenol and intermediates concentration in solution after the photolytic degradation. For clarity, intermediates are plotted in the left axis, and phenol is plotted in the right axis.

4.4.1.2. TiO_2 as photocatalyst

The photodegradation of phenol was also performed using TiO_2 as photocatalyst, aiming at increasing the efficiency of the removal, in terms of both phenol conversion and lower amount of degradation intermediates. The ecotoxicity was also measured for aliquots taken at 1, 3 and 6 hours, and the corresponding data is presented in Figure 4.9. First of all, it should be mentioned that it was not possible to measure the solutions after the photocatalytic process using TiO_2. Large dilution factors where needed in order to get measurable luminescence losses, which indicates the high toxicity of the solutions. Indeed, the decrease in the luminescent signal was so fast that the readings after 5 min of incubation were near zero (100% toxic). In order to work around this issue, dilution factors of about 8% were used.

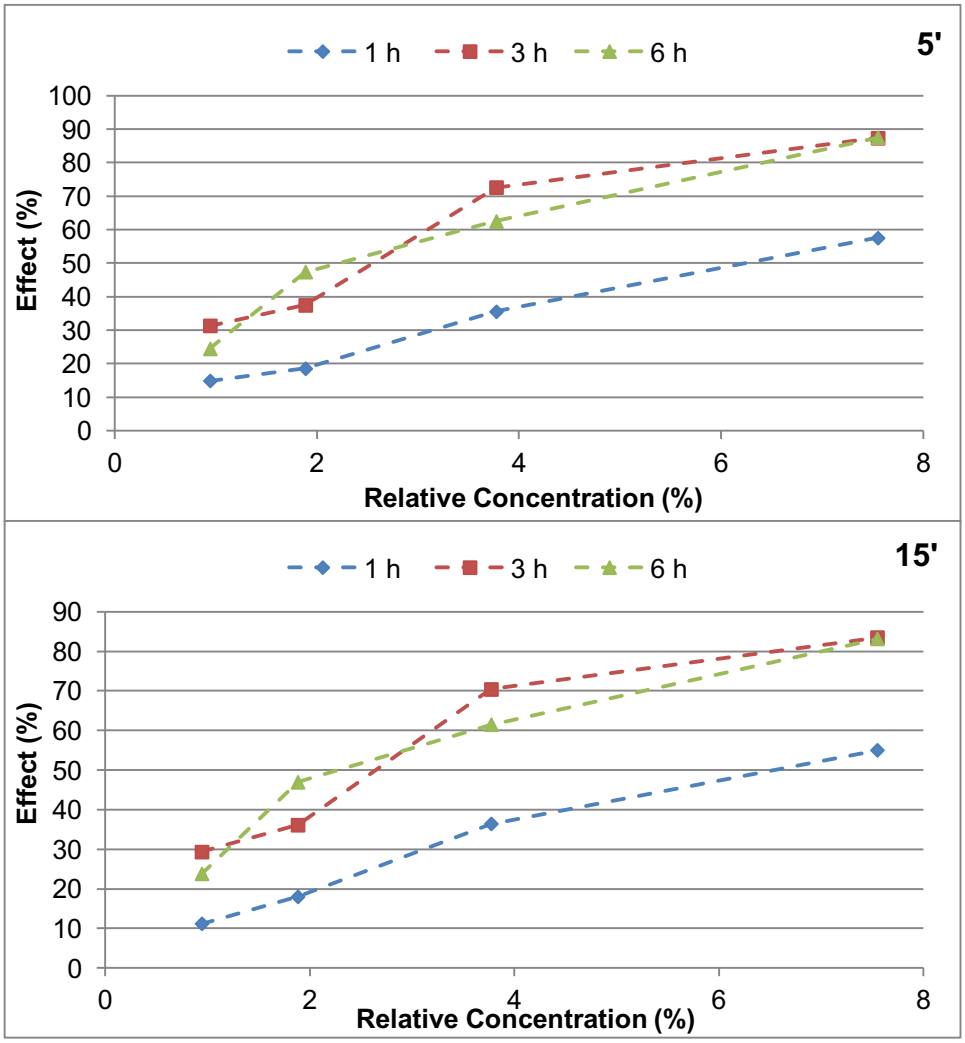

Figure 4.9 - Loss of bioluminescence signal after 5 and 15 min of incubation for the photodegradation of phenol using TiO_2 as photocatalyst, at various irradiation times (ca. 1, 3 and 6 h).

Thus, Figure 4.9 shows that when TiO_2 as used as photocatalyst, the toxicity of the solution increased with the irradiation time, suggesting that the mechanism of the photoassisted degradation reaction generates toxic intermediates that would gradually accumulate in the solution. Consequently, the final solution after 6 hours of irradiation in the presence of TiO_2 catalyst becomes more toxic that the initial one before the photocatalytic treatment.

In terms of phenol conversion and intermediates formation Figure 4.10,shows the evolution over time, where it can be observed that TiO_2 is a much more efficient photocatalyst compared to direct photolysis for the removal of phenol. For instance, phenol conversion ranged from 8, 27 and 56 % after 1, 3 and 6 hours or irradiation, respectively.

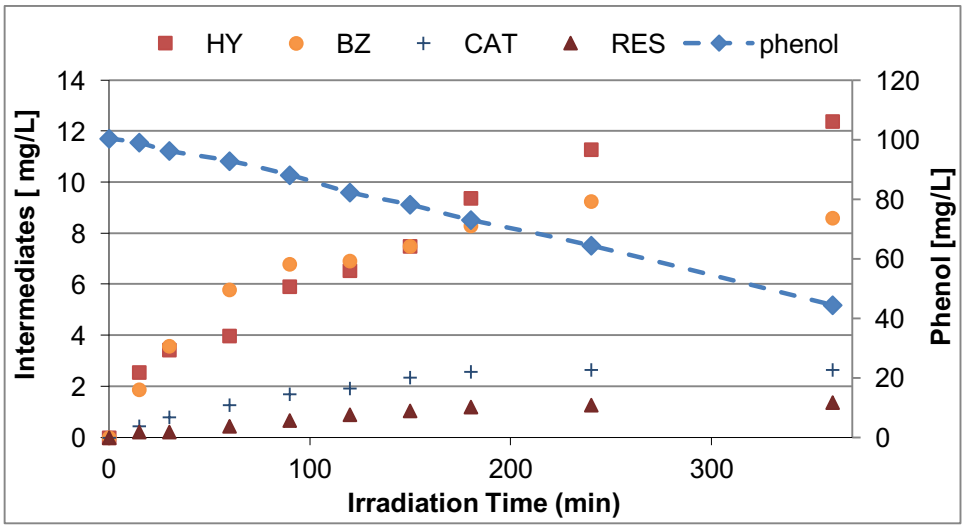

Figure 4.10 - Evolution of phenol and intermediates concentration in solution after the photolytic degradation using TiO_2 powders as photocatalyst. For clarity, intermediates are plotted in the left axis, and phenol is plotted in the right axis.

Despite phenol concentration gradually disappears with the photocatalytic treatment, the toxicity of the solution is much higher than that of the initial solution and even higher than that of the photolytic degradation (where the conversion of phenol was almost negligible). This is due to the nature and amount of intermediates formed during the photocatalytic degradation in the presence of TiO_2 powders. Indeed, as shown in Figure 4.10 when using titania as catalyst, the oxidation of phenol in para-position to form quinones (hydroquinone and benzoquinone) is predominant over the formation of catechol or resorcinol, which were detected in much lower amounts in the solution. Furthermore, the concentration of the quinones is increasing with the irradiation time and accumulates in the solution, indicating that, under these experimental conditions, the degradation of the intermediates does not take place.

As a result, the ecotoxicity of the treated solution is extremely high, even after 1 hours of irradiation (ca. concentration of quinones of 5 mg/L, whereas the EC_{50} values for these quinones was about 0.023-0.049, see Table 4.7).

4.4.1.3. Hybrid TiO_2/CQ as photocatalyst

The performance of a hybrid TiO_2/carbon composite as photocatalyst was investigated in terms of photocatalytic degradation and ecotoxicity, based on the previous results of ADPOR group reporting the beneficial effect of the incorporation of nanoporous carbons as additives to semiconductors for the degradation of phenolic compounds [Velasco, 2012b; Andrade, 2014; Carmona, 2015]. The obtained data regarding the bioluminescence assays is presented in Figure 4.11.

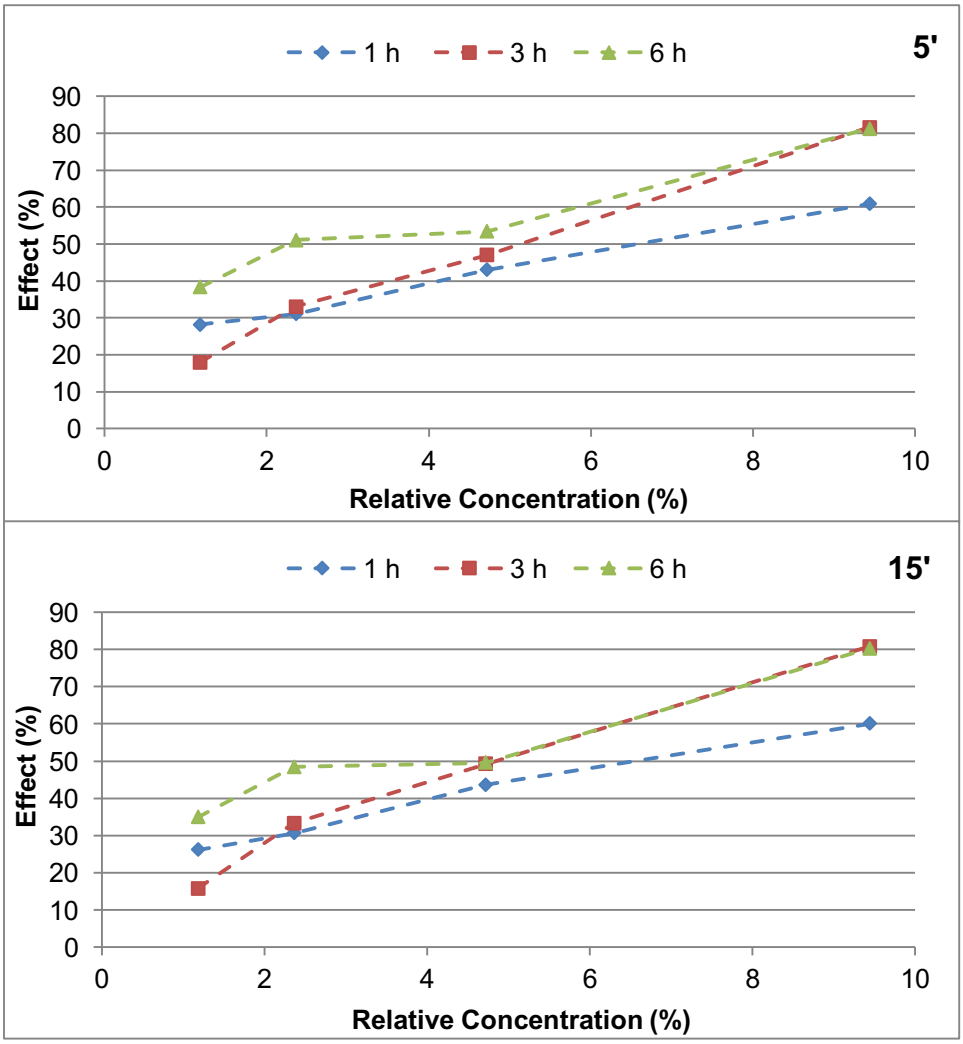

Figure 4.11 - Loss of bioluminescence signal after 5 and 15 min of incubation for the photodegradation of phenol using TiO_2/CQ hybrid composite as photocatalyst, at various irradiation times (ca. 1, 3 and 6 h).

As already found in the case of TiO_2, the large dilution factors were needed in order to record reliable readings of luminescence, indicating that the solution is quite toxic compared to the initial one. In this case, the initial dilution of the sample was ca. 0.1, slightly smaller than that of TiO_2, suggesting that the incorporation of the carbon additive has a beneficial effect on the final toxicity of the solution. Regarding the luminescence signal, data followed increasing patterns with the irradiation time, suggesting again that the solution becomes gradually more toxic after long irradiation times, likely due to the accumulation of the intermediates. This is more clearly seen in Figure 4.12, comparing the performance of the studied catalysts after various irradiation times.

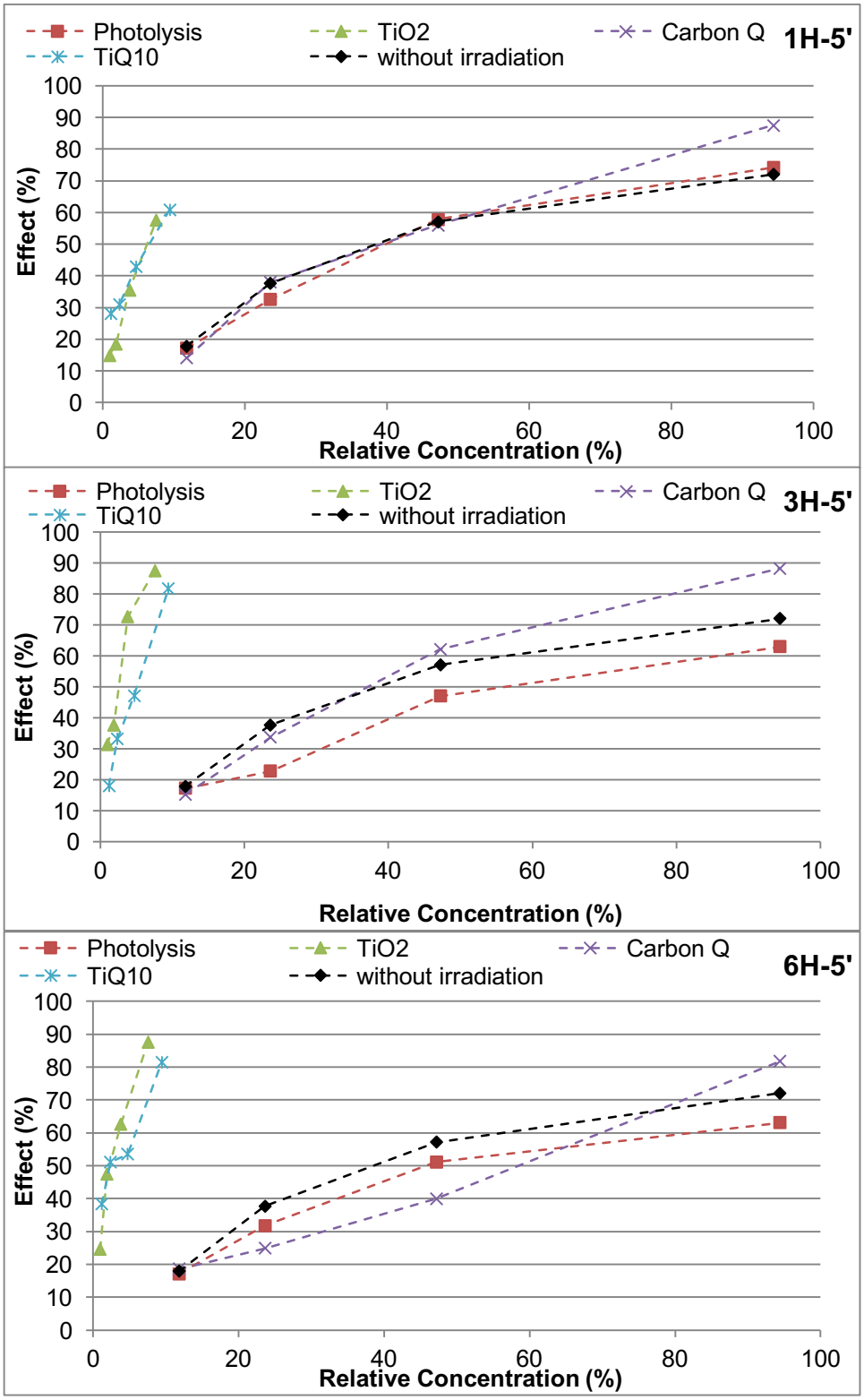

Figure 4.12. Comparison of the performance of the studied catalysts after various irradiation times.

To further corroborate this fact, the solution was analyzed by liquid chromatography, and the compounds identified and quantified as seen in Figure 4.13. Regarding phenol, the incorporation of the carbon additive increased slightly the conversion of phenol, already confirming the beneficial effect of the carbon material.

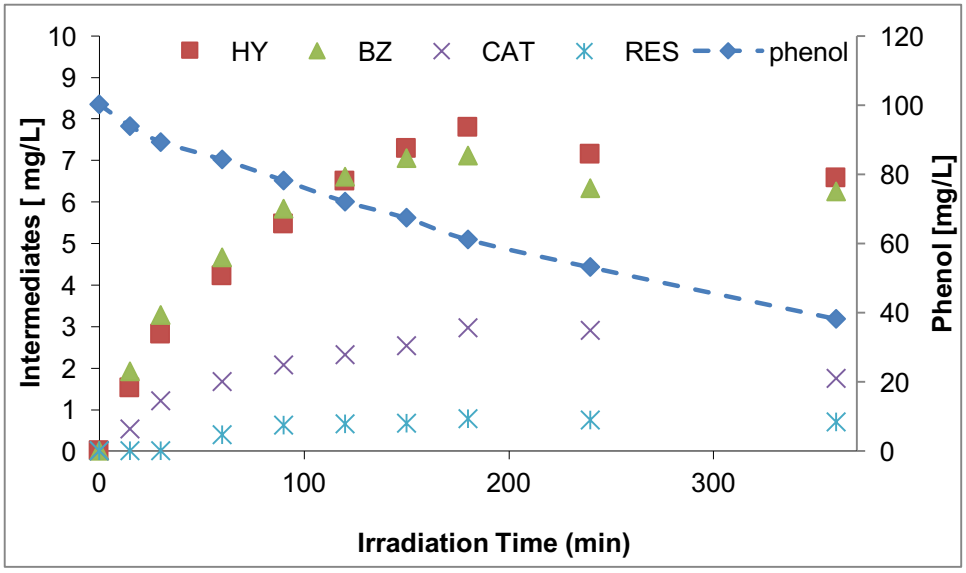

Figure 4.13. Evolution of phenol and intermediates concentration in solution after the photolytic degradation using TiO_2/nanoporous carbon composite as photocatalyst. For clarity, intermediates are plotted in the left axis, and phenol is plotted in the right axis.

It should be mentioned that due to the porosity of the TiO_2/carbon composite (inherited by the carbon material as discussed in section 4.1), the amount of phenol adsorbed in the porosity of the catalyst was also evaluated in dark conditions, to determine the extent of phenol removal due to adsorption and not to photodegradation. Data is also included in Figure 4.14 for clarity, and indicates that the amount of phenol retained in the porosity of the TiO_2/carbon composite accounts for ca. 7 % of phenol and stabilized after the first 30 minutes.

What is important to point out is that the adsorption process does not generate the oxidation of the pollutant, thus the detection of the intermediates is due to the photocatalytic process. As also shown in Figure 4.13, quinones are still the dominant intermediates formed during the photodegradation, however some differences are observed compared to the use of TiO_2 alone. The first one is that the amount of catechol increased in the presence of the carbon additive, indicating a regioselectivity towards the preferential oxidation in the *ortho*- position of the aromatic ring (over *para*- position in quinones). A similar trend had been observed for other semiconductor/carbon composites towards the degradation of phenol, as well as in the case of the use of nanoporous carbons alone as photocatalysts when using UV illumination [Velasco, 2012b; Andrade, 2014; Carmona, 2015]. This is important since according to literature, catechols are more reactive than quinones (due to the stability of intermediates formed), as a result of which the degradation pathway of catechol proceeds through a simple mechanism involving a less number of intermediates (organic acids) [Santos, 2002; Velasco, 2012b]

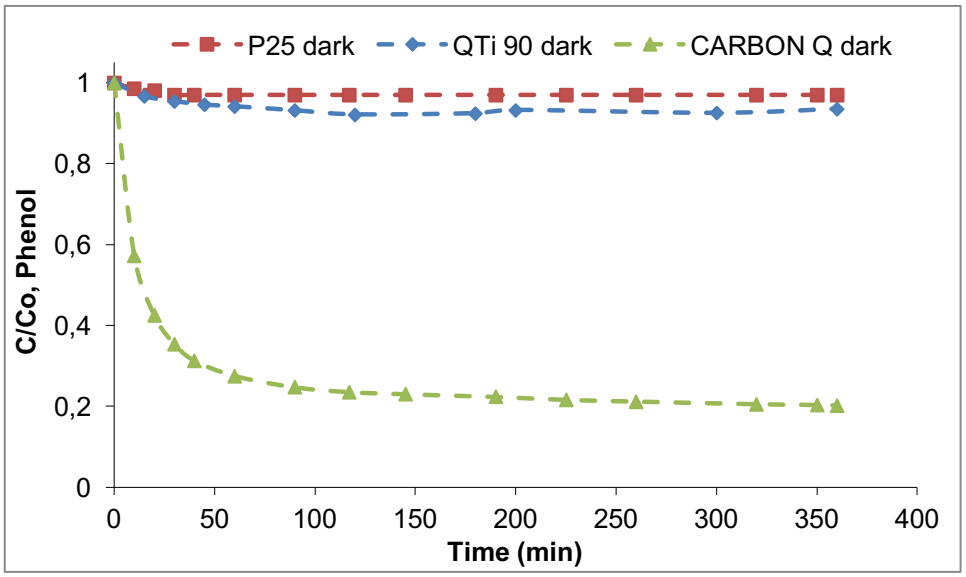

Figure 4.14 - Evolution of phenol concentration in solution under dark conditions with 3 studied catalysts, to evaluate the amount of phenol removed by adsorption.

The second difference concerns the amount of intermediates; in the presence of the carbon additive, a slight modification of the pattern is observed after 3-4 hours of illumination, with the concentration of quinones starting to decrease (as opposed to TiO_2). Overall, there are also more catechol and less quinones formed when the TiO_2/carbon photocatalyst is used. This suggests that not only phenol but also a fraction of the formed intermediates is degraded in the course of the photocatalytic runs. This has a marked impact in the ecotoxicity of the solution, which is lower when the hybrid TiO_2/carbon photocatalyst is used Figure 4.12.

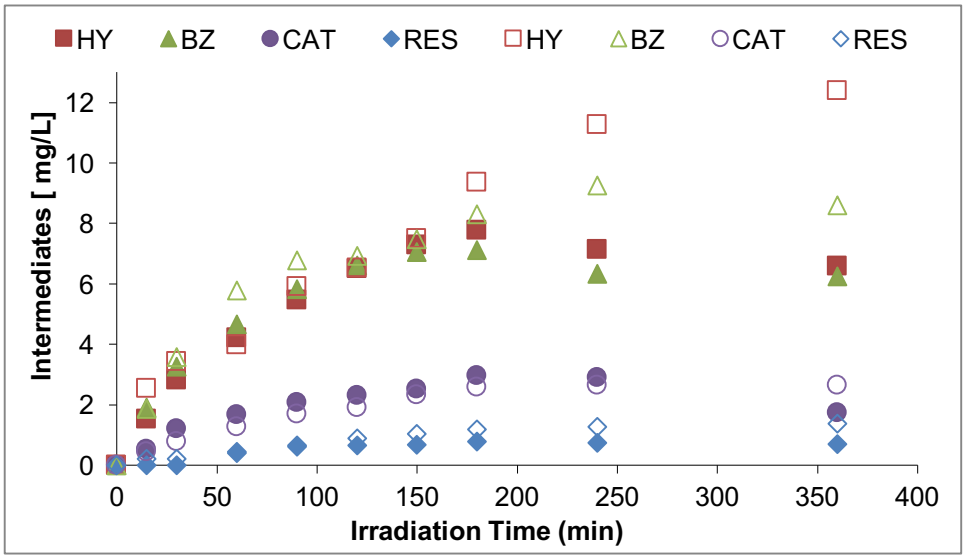

Figure 4.15. Evolution of phenol intermediates concentration in solution after the degradation using TiO_2 (empty symbols) and TiO_2/nanoporous carbon composite (filled symbols) as photocatalysts.

In sum, the incorporation of the carbon additive is able to gradually reduce the toxicity of the solution compared to TiO_2 after long in illumination times. However, values are still quite high based on the high luminescence losses, due to the predominance of quinones as intermediates. Further studies should be undertaken to explore the effect of the amount of carbon additive.

4.4.1.4. CQ as photocatalyst

We have also explored the role of the nanoporous carbon itself as photocatalyst. Based on the previous studies of ADPOR group, certain nanoporous carbons are capable of some degree of photoactivity when exposed to adequate illumination in aqueous suspensions, due to their ability to photogenerate radical species. In this master thesis, we have used the selected nanoporous carbon – sample CQ- as photocatalysts in the absence of a semiconductor, so as to determine its photoactivity under simulated solar light and the impact on ecotoxicity of the solution. The material was chosen based on previous studies of the group with this nanoporous carbon under UV irradiation [Velasco, 2012b].

As seen in Figure 4.16, the preliminary studies showed that when the nanoporous carbon was used as photocatalyst, the toxicity of the solution was much lower than that obtained when either TiO_2 or hybrid TiO_2/CQ composites where used. Also, the toxicity of the solution was also decreasing gradually with the irradiation time, reaching low toxicity values after 6 hours (even outperforming the photolytic reaction). The relative concentration for 50% effect after six hours was about 60% which is the best up to now. The maximum effect comparing with the catalyst TiO_2 is reduced by 20% for one and three hours and 30% in the six hour exposure.

In this case, due to the high porosity of the carbon material, the decrease in the ecotoxicity of the solution cannot be exclusively attributed to the photocatalytic reaction, but to the simultaneous adsorption on the porosity of the carbon material (see Figure 4.14). Thus, further studies need to be undertaken to clarify this issue.

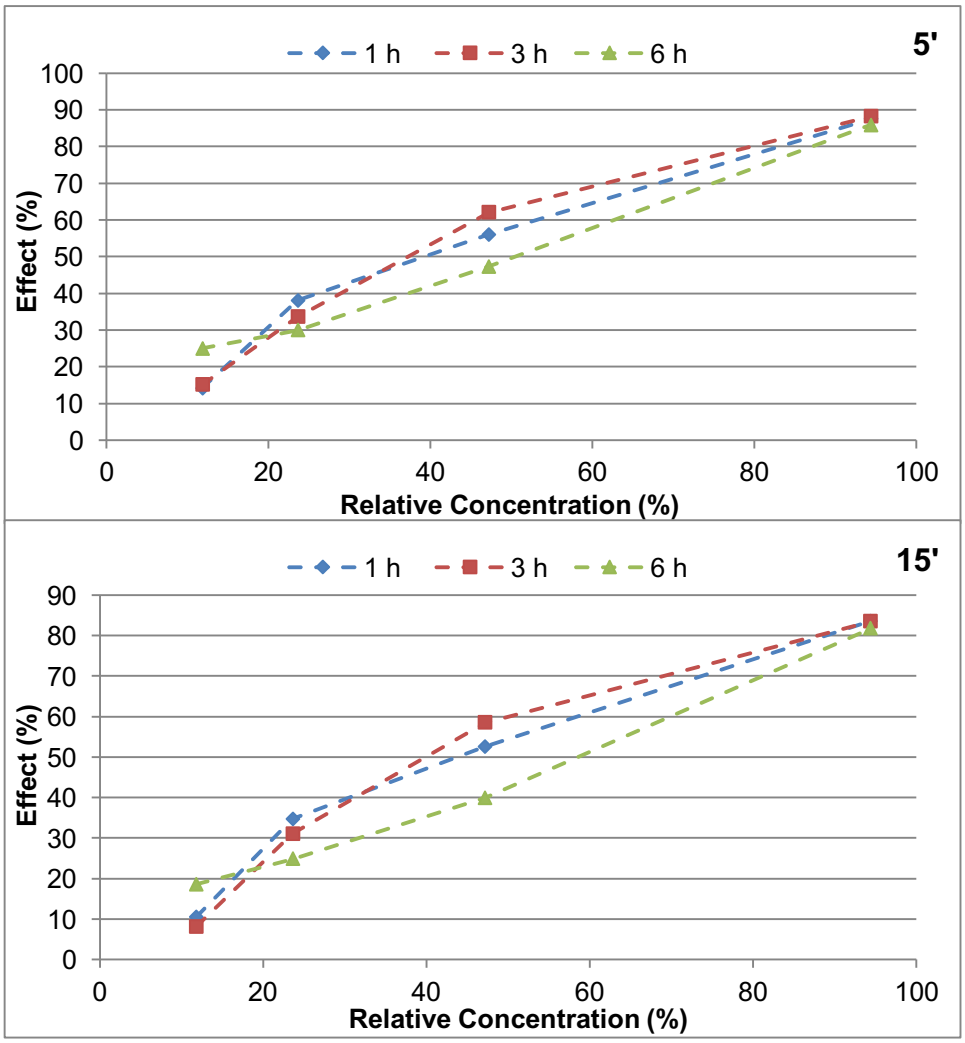

Figure 4.16 - Loss of bioluminescence signal after 5 and 15 min of incubation for the photodegradation of phenol using carbon CQ as photocatalyst at various irradiation times (ca. 1, 3 and 6 h).

4.5. Ecotoxicity measurements of industrial wastewater

An important objective of this work was to investigate the ecotoxicity of wastewater from industrial origin - typically more complex water matrices compared to synthetic solutions-, as well as the impact of various photocatalytic processes on the evolution of the toxicity itself. Selected parameters of the composition of the wastewater are detailed in the experimental section Table 3.1.

Before the photocatalytic runs, the ecotoxicity of the as-received wastewater was measured; data obtained is shown in Figure 4.17 for 5 and 15 min of exposure. The wastewater from industrial origin is more toxic than the synthetic phenol solutions herein prepared; this was rather expected considering that other than phenolic compounds (ca. 4.2 mg/L total phenols), the water is characterized by a high ionic conductivity (1067 microS/cm at 20ºC) and a Total Organic Carbon content of 291 mg/L.

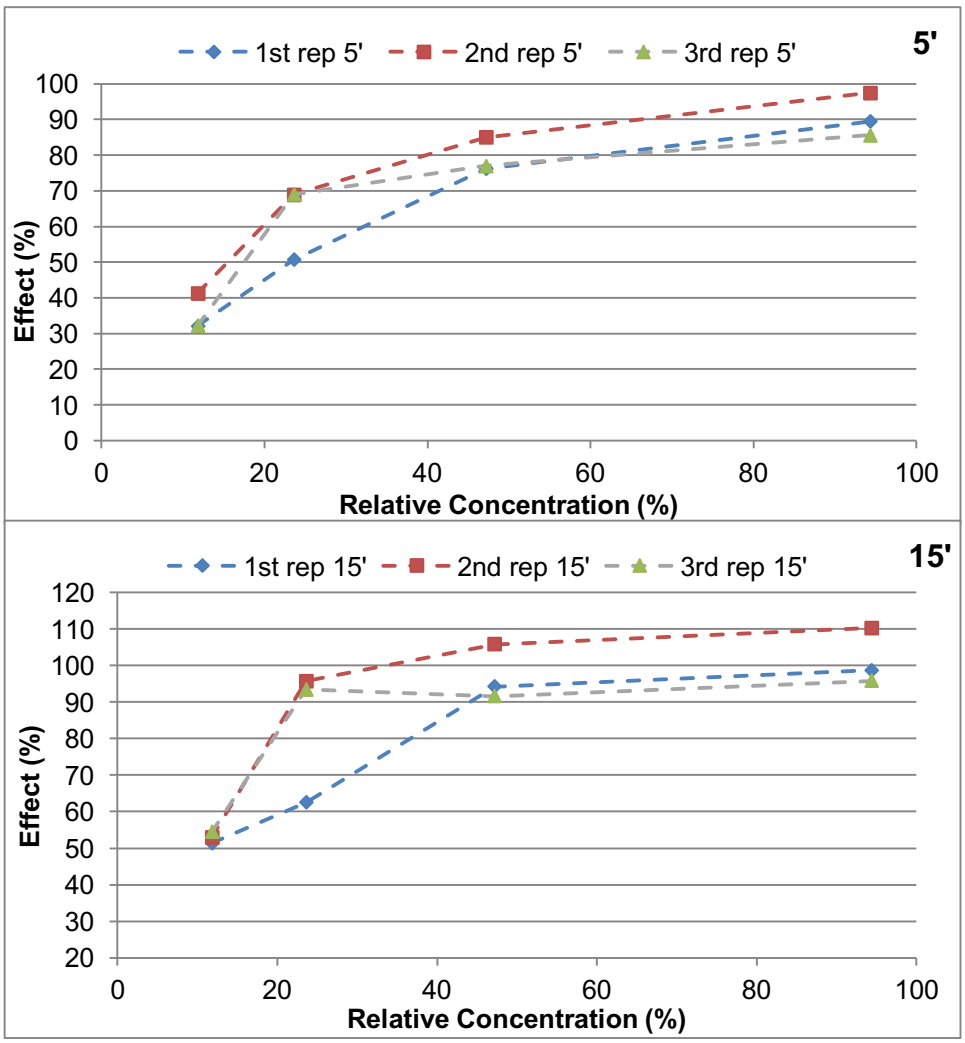

Figure 4.17 Loss of bioluminescence signal after 5 and 15 min of incubation in the as-received wastewater.

Interestingly, the incubation time showed a difference compared to the synthetic samples, since the toxicity increased from 5 to 15 min of incubation of the bacteria. This suggests that the mechanism of inhibition of the luminescence signal follows a slower kinetics in a complex water matrix.

4.5.1.1. Impact of photodegradation assays on the toxicity of the industrial wastewater

Figure 4.18 shows the comparison of the bioluminescence assays obtained for the industrial wastewater with the different photocatalysts used. The corresponding individual plots can be found in Annex B. Most interestingly, as a general trend, all the photocatalytic processes applied with the exception of the use of TiO_2 as photocatalyst) decreased significantly the toxicity of the solution, even after 1 hour of irradiation. The effect was more pronounced after 6 hours of irradiation. Most performing photocatalysts were carbon Q, with better results in terms of final toxicity than the photolytic degradation or the catalysts incorporating TiO_2 as semiconductor.

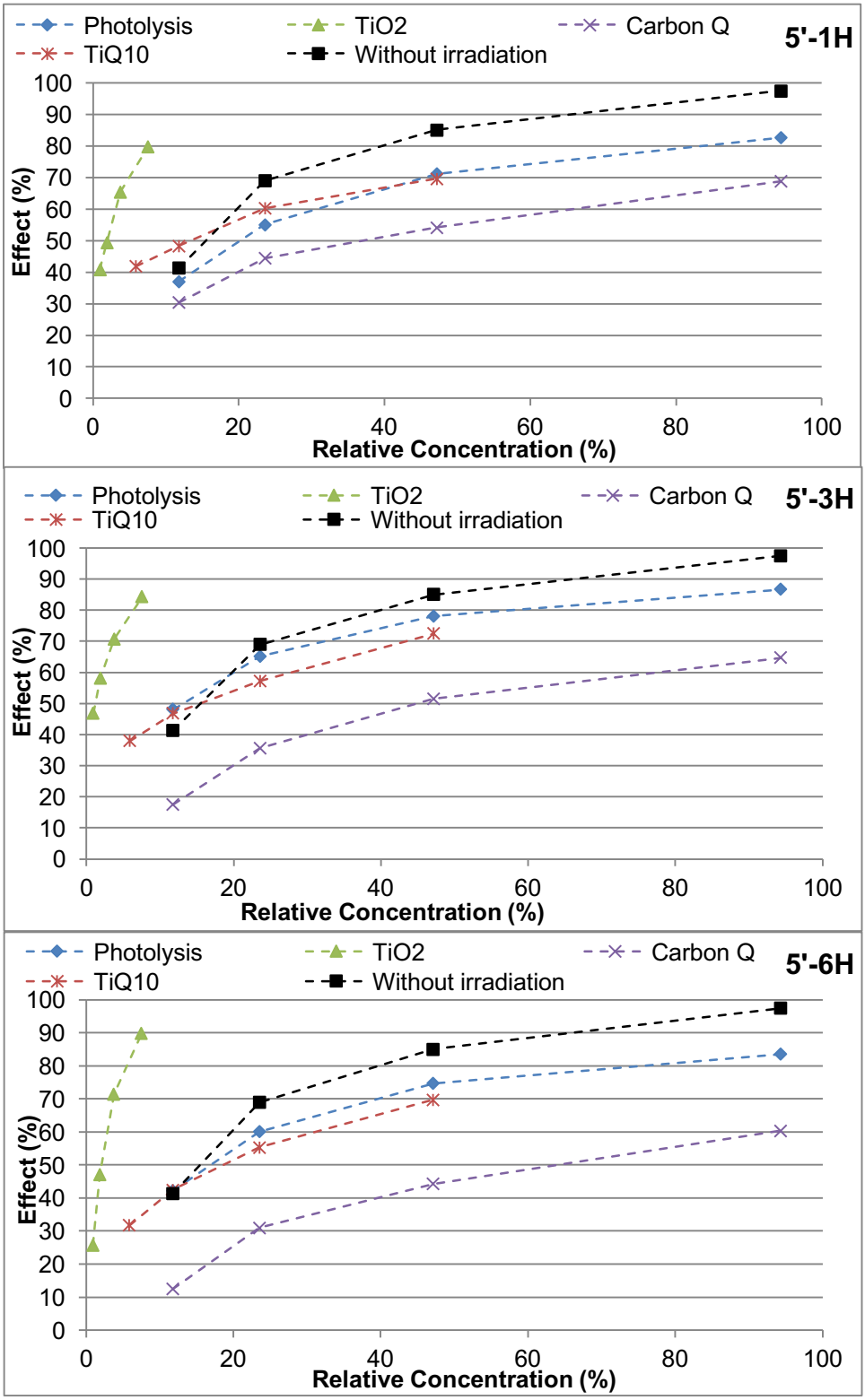

Figure 4.18 - Comparative loss of bioluminescence signal after 5 min of incubation for the photodegradation of the industrial wastewater using different photocatalyst and at various irradiation times (ca. 1, 3 and 6 h).

This is most outstanding since the irradiation source was simulated solar light, thus better (or even faster) results might be expected if more energetic light source (i.e., UV light) is applied.

It is also interesting to point out that the beneficial impact of the carbon additive to TiO_2 was more evident for this complex wastewater than in the case of the synthetic solutions. As seen, the incorporation of ca. 10 wt.% of the carbon material to the hybrid photocatalyst resulted in a faster evolution of the ecotoxicity of the resulting solution, even after 1 hour of irradiation.

Although further studies should be undertaken to clarify this behavior and to discriminate the exact role of the nanoporous carbon as photocatalyst and adsorbent, as well as the exact nature of the intermediates formed and the other species present in the water, these results are most promising considering that he toxicity of the water was significantly reduced after 1 hour of irradiation using visible light.

Chapter

5. Conclusions

This thesis presents the results of an ecotoxicity study of synthetic and real wastewater containing phenolic compounds from industrial origin, after photolysis and photocatalytic degradation using TiO_2 and a nanoporous carbon in the formulation of the photocatalyst (the later as catalyst itself and as additive to TiO_2) using simulated solar light. The main conclusions of this study are presented below:

- An optimized protocol allowed the determination of EC_{50} values using the inhibition bioluminescence assay of *Vibrio fischeri* for the synthetic and real wastewater. The conditions were:
    - pH adjustment of water aliquots -with NaOH or HCl- between 6 and 8;
    - time of incubation of 5 and 15 minutes;
    - samples prepared in distilled, deionized water;
    - measurements of fresh solution up to 72 h after their preparation.
    - In real wastewater, the incubation time played an important role, with toxicity values increasing from 5 to 15 min of incubation of the bacteria. This suggests that the mechanism of inhibition of the luminescence signal follows a slower kinetics in complex water matrices.
- The results about EC_{50} values of various phenolic compounds revealed that single component solutions (synthetic) of phenol presented moderated ecotoxicity values, similar to those reported in the literature (ca. EC_{50} 5' $\simeq$ [19 – 20] mg/L and EC_{50} 15' $\simeq$ [21 – 23] mg/L) for phenol concentrations of 100 ppm. The ecotoxicity of the main phenol degradation intermediates (i.e., catechol, benzoquinone, hydroquinone, resorcinol) was also evaluated from single component synthetic solutions. Data showed higher ecotoxicity values for most intermediates than phenol itself, with the exception of catechol.
- Regarding the use of photoassisted reactions as advanced oxidation processes for the degradation of phenolic solutions, different trends were obtained upon the use (or not) of the catalyst and its nature, for both the synthetic and real water samples.
    - When no catalyst is used (photolytic reaction), the toxicity did not changed due to the low photodegradation yields achieved (ca. 3%).
    - The use of TiO_2-based photocatalysts improved the photodegradation yield in terms of phenol conversion in synthetic solutions, but the solutions were much more toxic, due to the accumulation of quinones as main intermediates.
    - The best photocatalysts, in terms of lower toxicity were those incorporating the nanoporous carbon in the formulation (either TiO_2-free of TiO_2/carbon hybrid composites). In the case of the use of bare carbon Q, more information is needed about the photodegradation yield and the nature of the intermediates to support this observation, to discriminate the role of the photochemical activity of the nanoporous carbon and that of the simultaneous adsorption on the porosity.
- With the exception of TiO_2, the toxicity of the real wastewater solution decreased meaningfully when a photocatalyst was used, even after 1 hour of irradiation. The effect was more pronounced after 6 hours of irradiation. Furthermore, the toxicity of the pristine solution increased when bare TiO_2 powders were used as photocatalyst, and decreased for

the photolytic reaction and the hybrid TiO_2/carbon composite, being the effect more pronounced for the nanoporous carbon alone. In this regard, again further studies are need to discriminate the origin of this behavior since various phenomena might be taking place simultaneously (adsorption and photodegradation) in the pores of the carbon.

In sum, it may be concluded that these results are very promising since the irradiation source was simulated solar light and the toxicity of the water was significantly reduced even after 1 hour of irradiation using visible light.

It should also be mentioned that further studies would be needed to pursue the work, with main activities focusing on:

- Discriminating the exact role of the nanoporous carbon as photocatalyst and adsorbent with various carbon loading ratios.
- Exploring the use of more energetic light source (i.e., UV light), in order to obtain better photodegradation yields.
- Extending the study to other nanoporous carbons with different textural and chemical properties, and analyzing both the ecotoxicity after the photocatalytic degradation process, and the photooxidation yield in terms of pollutant conversion and mineralization.

Chapter

6. References

References

Allard, B., Craun, G. F., Oude, N. T., Falkenmark, M., Golterman, H. L., Lindstrom, T., & Piver, W. T. (1991) *Environmental Chemistry - Water Pollution*. Edited by O. Hutzinger. Bayreuth: Springer-Verlag Berlin Heidelberg GmbH. doi: 10.1007/978-3-540-46685-7.

Alyssa, H. (1997) *Four Systems of Our Earth - Earth Science - Hydrosphere*. Available at: https://pt.slideshare.net/Alyssa10/earth-science-hydrosphere-ppt (Accessed: 10 June 2017).

Andrade, M. A., Carmona, R. J., Mestre, A. S., Matos, J., Carvalho, A. P., and Ania, C. O. (2014) 'Visible light driven photooxidation of phenol on TiO2/Cu-loaded carbon catalysts', *Carbon*. Elsevier Ltd, 76, pp. 183–192. doi: 10.1016/j.carbon.2014.04.066.

Andrade, M. A., Mestre, A. S., Carmona, R. J., Carvalho, A. P., and Ania, C. O. (2015) 'Effect of the irradiation wavelength on the performance of nanoporous carbon as an additive to TiO2', *Applied Catalysis A: General*. Elsevier B.V., 507, pp. 91–98. doi: 10.1016/j.apcata.2015.09.036.

Ania, C. O., Cabal, B., Pevida, C., Arenillas, A., Parra, J. B., Rubiera, F., and Pis, J. J. (2007) 'Removal of naphthalene from aqueous solution on chemically modified activated carbons', *Water Research*, 41(2), pp. 333–340. doi: 10.1016/j.watres.2006.10.016.

AQUASTAT (2016) *Food and Agriculture Organization of the United Nations*. Available at: http://www.fao.org/nr/water/aquastat/water_use/index.stm (Accessed: 17 July 2017).

AZUR Environmental (1998) *Microtox Acute Toxicity Test*. Available at: http://www.coastalbio.com/images/Acute_Overview.pdf (Accessed: 8 March 2017).

Baruah, J. B. (2011) *Chemistry of Phenolic Compounds: STATE OF THE ART*. New York: Nova Science Publishers.

Bayarri, B., M.N.Abellan, Gimenez, J., and Esplugas, S. (2007) 'Selected Contributions of the 4th European Meeting on Solar Chemistry and Photocatalysis: Environmental Applications', *Catalysis Today*, 129, pp. 1–262.

Bendary, E., Francis, R. R., Ali, H. M. G., Sarwat, M. I., and El Hady, S. (2013) 'Antioxidant and structure–activity relationships (SARs) of some phenolic and anilines compounds', *Annals of Agricultural Sciences*. Faculty of Agriculture, Ain Shams University, 58(2), pp. 173–181. doi: 10.1016/j.aoas.2013.07.002.

Biscarini, C. and Ubertini, L. (2017) *Overview of the Case Studies extracted from the World Water Development Report 2017*.

Blaise, C. and Férard, J. F. (2005) 'SMALL-SCALE FRESHWATER TOXICITY INVESTIGATIONS', in. Netherlands: Springer, p. (69-125) 563.

Blum, D. and Speece, R. (1991) 'A Database of Chemical Toxicity to Environmental Bacteria and Its Use in Interspecies Comparisons and Correlations', *Research Journal of the Water Pollution Control Federation*, 63(3), pp. 198–207. doi: 10.2307/25043983.

Boyd, E. M., Meharg, A. A., Wright, J., and Killham, K. (1997) 'Assessment of toxicological interactions of benzene and its primary degradation products (catechol and phenol) using a lux-modified

bacterial bioassay', *Environmental Toxicology and Chemistry*, 16(5), pp. 849–856. doi: 10.1897/1551-5028(1997)016<0849:AOTIOB>2.3.CO;2.

Braslavsky S.E. (2007) 'Glossary of terms used in photochemistry 3rd edition (IUPAC Recommendations 2006)', *Pure Appl. Chem*, pp. 79, 293–465.

Brunauer, S., Deming, L. S., Deming, W. E., and Teller, E. (1940) 'On a Theory of the van der Waals Adsorption of Gases', *Journal of the American Chemical Society*, 62(7), pp. 1723–1732. doi: 10.1021/ja01864a025.

Carmona, R. J., Velasco, L. F., Hidalgo, M. C., Navío, J. A., and Ania, C. O. (2015) 'Boosting the visible-light photoactivity of Bi2WO6 using acidic carbon additives', *Applied Catalysis A: General*. Elsevier B.V., 505, pp. 467–477. doi: 10.1016/j.apcata.2015.05.011.

Carmona, R. J., Velasco, L. F., Laurenti, E., Maurino, V., and Ania, C. O. (2016) 'Carbon Materials as Additives to WO3 for an Enhanced Conversion of Simulated Solar Light', *Frontiers in Materials*, 3(February), p. 9. doi: 10.3389/FMATS.2016.00009.

Cho, Y, Choi, W, Lee, C-H., Hyeon, T., (2001) 'Visible Light-Induced Degradation of Carbon Tetrachloride on', *Environ. Sci. Technol.*, 35(5), pp. 966–970.

Cordero-Garci-a, A., Guzmán-Mar, J. L., Hinojosa-Reyes, L., Ruiz-Ruiz, E., and Hernández-Ramírez, A. (2016) 'Effect of carbon doping on WO3/TiO2 coupled oxide and its photocatalytic activity on diclofenac degradation', *Ceramics International*. Elsevier, 42(8), pp. 9796–9803. doi: 10.1016/j.ceramint.2016.03.073.

Crawford, J., Faroon, O., Wilson, J., Llados, F. T., Garber, K., Paikoff, S. J., and Lumpkin, M. H. (2006) 'Potencial for human exposure', *Toxicological Profile for Phenol*. Georgia, pp. 149–172.

E-PRTR (2015) *Environmental data from industrial facilities in European Union Member States*. Available at: http://prtr.ec.europa.eu/#/home (Accessed: 5 September 2017).

Falkenmark, M. and Rockström, J. (2004) *Balancing Water for Humans and Nature: The New Approach in Ecohydrology*, *Earthscan*.

Faria, J. L. and Wang, W. (2009) *Carbon materials in photocatalysis (Ch. 13), in Carbon Materials for Catalysis*. Edited by P. Serp and J. L. Figueiredo. New Jersey: Wiley & Sons.

Figini-Albisetti, A., Velasco, L. F., Parra, J. B., and Ania, C. O. (2010) 'Effect of outgassing temperature on the performance of porous materials', *Applied Surface Science*, 256(17), pp. 5182–5186. doi: 10.1016/j.apsusc.2009.12.090.

Gaudet, I. D. (1994) *Standard Procedure for MICROTOX analysis*. Alberta.

Germán, B., Gloria, M. and Moreno-Andrade, I. (2009) 'Eliminación biológica de altas concentraciones de fenol presente en aguas residuales', *AIDIS*, pp. 1–7.

Gomes, A. I. de E. (2007) *Avaliação da Ecotoxicidade de Águas Superficiais Aplicação à Bacia Hidrográfica do Rio Leça*, *Revista Brasileira de Terapia Intensiva*. FACULDADE DE ENGENHARIA DA UNIVERSIDADE DO PORTO. doi: 10.1590/S0103-507X2007000100019.

Gomis-Berenguer, A., Celorrio, V., Iniesta, J., Fermin, D. J., and Ania, C. O. (2016) 'Nanoporous carbon/WO3 anodes for an enhanced water photooxidation', *Carbon*. Elsevier Ltd, 108, pp. 471–479. doi: 10.1016/j.carbon.2016.07.045.

Gomis-Berenguer, A., Velasco, L. F., Velo-Gala, I., and Ania, C. O. (2017) 'Photochemistry of nanoporous carbons: Perspectives in energy conversion and environmental remediation', *Journal of Colloid and Interface Science*, 490, pp. 879–901. doi: 10.1016/j.jcis.2016.11.046.

Green, M. A., Ho-Baillie, A. and Snaith, H. J. (2014) 'The emergence of perovskite solar cells', *Nature Photonics*. Nature Publishing Group, 8(7), pp. 506–514. doi: 10.1038/nphoton.2014.134.

Grzechulska, J. and Morawski, A. (2003) 'Photocatalytic labyrinth flow reactor with immobilized P25 TiO2 bed for removal of phenol from water', *Applied Catalysis B: Environmental*, 46(2), pp. 415–419.

Guillot, A. and Stoeckli, F. (2001) 'Reference isotherm for high pressure adsorption of CO2 by carbons at 273 K', *Carbon*, 39(13), pp. 2059–2064. doi: 10.1016/S0008-6223(01)00022-7.

Han, F., Kambala, V. S. R., Srinivasan, M., Rajarathnam, D., and Naidu, R. (2009) 'Tailored titanium dioxide photocatalysts for the degradation of organic dyes in wastewater treatment: A review', *Applied Catalysis A: General*, 359(1–2), pp. 25–40. doi: 10.1016/j.apcata.2009.02.043.

Haro, M., Velasco, L. F. and Ania, C. O. (2012) 'Carbon-mediated photoinduced reactions as a key factor in the photocatalytic performance of C/TiO2', *Catalysis Science and Technology*, 2(11), p. 2264. doi: 10.1039/c2cy20270k.

Hoeben, W. F. L. M. (2000) *Pulsed corona-induced degradation of organic materials in water*. Technische Universiteit Eindhoven. doi: 10.6100/IR535691.

Idowu, S. O. (2009) *World Business Council for Sustainable Development*.

Kahru A, Kurvet M and Kulm I (1996) 'Toxicity of phenolic wastewater to luminescent bacteria Photobacterium phosphoreum and activated sludges', *Water Sci Technol*, p. 33(6):139– 46.

Kaiser, M. (1998) 'Significance of Bottom-Fishing Disturbance', *Conservation Biology*, 12(6), pp. 1230–1235. doi: 10.1046/j.1523-1739.1998.0120061230.x.

Kay, B. (1999) *Water Resources: Health, Environment and Development*. Edited by E & FN Spon. London: Routledge.

Khehra, M. S., Saini, H. S., Sharma, D. K., Chadha, B. S., and Chimni, S. S. (2006) 'Biodegradation of azo dye C.I. Acid Red 88 by an anoxic - Aerobic sequential bioreactor', *Dyes and Pigments*, 70(1), pp. 1–7. doi: 10.1016/j.dyepig.2004.12.021.

Klaassen, C. D. and Watkins, J. B. (2012) *Fundamentos em Toxicologia de Casarett e Doull*. Second edi. Edited by McGraw-Hill. Porto Alegre: AMGH.

Kubelka, P. and Munk, F. (1931) 'Ein Bitrag Zur Optik der Farbanstriche', *Z. Tech. Phys.*, (12), pp. 593–601.

Leary, R. and Westwood, A. (2011) 'Carbonaceous nanomaterials for the enhancement of TiO2 photocatalysis', *Carbon*, 49(3), pp. 741–772. doi: 10.1016/j.carbon.2010.10.010.

Lehr, J., Keeley, J., Lehr, J., and Kingery, T. (2005) *Domestic, Municipal, and Industrial Water Supply and Waste Disposal*. Edited by J. Lehr and J. Keeley. New Jersey: Wiley-interscience.

Lichtfouse, E., Robert, D. and Schwarzbauer, J. (2005) *Environmental Chemistry: Green Chemistry and Pollutants in Ecosystems*. Edited by D. Robert and J. Schwarzbauer. Springer.

Lips, C., Jelenic, M., Graham, S., and Ludwick, R. (2010) *The World Bank Annual Report*. Washington, D.C. doi: 10.1596/978-0-8213-8376-6.

López, R. and Gómez, R. (2012) 'Band-gap energy estimation from diffuse reflectance measurements on sol-gel and commercial TiO 2: A comparative study', *Journal of Sol-Gel Science and Technology*, 61(1), pp. 1–7. doi: 10.1007/s10971-011-2582-9.

Lucas, M. S., Dias, A. A., Sampaio, A., Amaral, C., and Peres, J. A. (2007) 'Degradation of a textile reactive Azo dye by a combined chemical-biological process: Fenton's reagent-yeast', *Water Research*, 41(5), pp. 1103–1109. doi: 10.1016/j.watres.2006.12.013.

Maçaira, J., Andrade, L. and Mendes, A. (2013) 'Review on nanostructured photoelectrodes for next generation dye-sensitized solar cells', *Renewable and Sustainable Energy Reviews*. Elsevier, 27(2013), pp. 334–349. doi: 10.1016/j.rser.2013.07.011.

Malinkiewicz, O., Yella, A., Lee, Y. H., Espallargas, G. M., Graetzel, M., Nazeeruddin, M. K., and Bolink, H. J. (2013) 'Perovskite solar cells employing organic charge-transport layers', *Nature Photonics*, 8(2), pp. 128–132. doi: 10.1038/nphoton.2013.341.

Margaux (2012) *World resources SIM center*. Available at: http://www.wrsc.org/attach_image/global-water-consumption-1900-2025 (Accessed: 28 July 2017).

Matos, J., García, A. and Poon, P. S. (2010) 'Environmental green chemistry applications of nanoporous carbons', *Journal of Materials Science*, 45(18), pp. 4934–4944. doi: 10.1007/s10853-009-4184-2.

Matos, J., Laine, J. and Herrmann, J. M. (1998) 'Synergy effect in the photocatalytic degradation of phenol on a suspended mixture of titania and activated carbon', *Applied Catalysis B: Environmental*, 18(3–4), pp. 281–291. doi: 10.1016/S0926-3373(98)00051-4.

Merck Index (2010). RSC Publishing. Available at: https://www.rsc.org/merck-index (Accessed: 5 September 2017).

Microbics Corporation (2010) 'MICROTOX ® TOXICITY TEST'. Kwai Chung: ALS Technichem, p. 1.

Minero, C., Mariella, G., Maurino, V., and Pelizzetti, E. (2000) 'Photocatalytic Transformation of Organic Compounds in the Presence of Inorganic Anions. 1. Hydroxyl-Mediated and Direct Electron-Transfer Reactions of Phenol on a Titanium Dioxide−Fluoride System', *Langmuir*, 16(6), pp. 2632–2641. doi: 10.1021/la9903301.

ModerWater (2012) 'Industry-leading toxicity detection'. New Castle: Modern Water Inc, November

(Microtox®M500), pp. 1–4.

Nadolna, J. and Zaleska, A. (2012) 'Mechanism of phenol photodegradation in the presence of pure and modified-TiO2: A review', *Water Research*, 46(17), pp. 5453–5471. doi: 10.1016/j.watres.2012.07.048.

Nagaveni, K., Hegde, M. S., Ravishankar, N., G. Subbanna, N., and Madras, G. (2004) 'Synthesis and structure of nanocrystalline TiO2 with lower band gap showing high photocatalytic activity.', *American Chemical Society*, 20 (7), pp. 2900–2907. doi: 10.1021/la035777v.

Olguin-Lora, P., Puig-Grajales, L. and Razo-Flores, E. (2003) 'Inhibition of the acetoclastic methanogenic activity by phenol and alkyl phenols', *Environmental Technology*, 24(8), pp. 999–1006. doi: 10.1080/09593330309385638.

Parra, J. B., Sousa, J. C. De, Bansal, R. C., Pis, J. J., and Pajares, J. A. (1995) 'Characterization of Activated Carbons by the BET Equation — An Alternative Approach', *Adsorpt. Sci. Technol.*, (12), pp. 51–66. doi: https://doi.org/10.1177/026361749501200106.

Parveza, S., Venkataraman, C. and Mukherjia, S. (2006) 'A review on advantages of implementing luminescence inhibition test (Vibrio fischeri) for acute toxicity prediction of chemicals', *Environment International*, pp. 265–268.

Pelizzetti E., Serpone N. Photocatalysis: Fundamental and applications. Wiley-Interscience. (1989). ISBN: 978-0-471-62603-9.

Pérez, A. R. (2014) 'Efecto de los compuestos de las aguas residuales de coquería en la degradación biológica de tiocianato (I)'. Acciona Agua, pp. 28–36.

PRTR-ES (2015) *Información pública de fuentes puntuales*. Available at: http://www.prtr-es.es/informes/pollutant.aspx (Accessed: 5 September 2017).

Raghu, S., Ahmed Basha, C. (2007) 'Chemical or electrochemical techniques, followed by ion exchange, for recycle of textile dye wastewater', *Journal of Hazardous Materials*, 149(2), pp. 324–330. doi: 10.1016/j.jhazmat.2007.03.087.

Rappoport, Z (2003) *The chemistry of phenols*, *The Chemistry of Phenols*. Edited by R. Z. John Wiley & Sons. doi: 10.1002/chin.200515296.

Rouquerol, J., Rouquerol, F., Llewellyn, P., Maurin, G., and Sing, K. S. W. (2014) *Adsorption by powders and porous solids. Principles, methodology and applications*. 2nd editio. London: Academic Press.

Ruz, C. (2011) *The Guardian*. Available at: https://www.theguardian.com/environment /blog/2011/oct/31/six-natural-resources-population (Accessed: 29 June 2017).

Santos, A., Yustos, P., Quintanilla, A., Rodríguez, S., and García-Ochoa, F. (2002) 'Route of the catalytic oxidation of phenol in aqueous phase', *Applied Catalysis B: Environmental*, 39(2), pp. 97–113. doi: 10.1016/S0926-3373(02)00087-5.

Santos, A., Yustos, P., Quintanilla, A., García-Ochoa, F., Casas, J. A., and Rodriguez, J. J. (2004)

'Evolution of Toxicity upon Wet Catalytic Oxidation of Phenol', *Environmental Science and Technology*, 38(1), pp. 133–138. doi: 10.1021/es030476t.

Shannon, M. A., Bohn, P. W., Elimelech, M., Georgiadis, J. G., Mariñas, B. J., and Mayes, A. M. (2008) 'Science and technology for water purification in the coming decades', *Nature*, p. 452 (7185), 301-310.

Sing, K. S. W., Everett, D. H., Haul, R. a. W., Moscou, L., Pierotti, R. a., Rouquérol, J., and Siemieniewska, T. (1985) 'INTERNATIONAL UNION OF PURE AND APPLIED CHEMISTRYCOMMISSION ON COLLOID AND SURFACE CHEMISTRY INCLUDING CATALYSIS. REPORTING PHYSISORPTION DATA FOR GAS / SOLID SYSTEMS with Special Reference to the Determination of Surface Area and Porosity', *Pure Appl. Chem.*, 54(11), pp. 603–619. doi: 10.1351/pac198557040603.

Soto, W. and Gutierrez, J. (2009) 'Salinity and Temperature Effects on Physiological Responses of Vibrio fischeri from Diverse Ecological Niches', *Microb Ecol*.

Spencer, T. and Altman, P. (2010) *Water facts: Climate Change, Water, and Risk*, *Natural Resources Defense Council*.

Sperling, M. (2007) *Wastewater Characteristics, Treatment and Disposal*. One. Edited by I. Aptara Inc., New Delhi. London: IWA Publishing - Alliance House.

SSWM (2012) *Sustainable Sanitation and Water Management*. Available at: http://www.sswm.info/content/reuse-water-between-businesses (Accessed: 28 July 2017).

Stranks, S. D. and Snaith, H. J. (2015) 'Metal-halide perovskites for photovoltaic and light-emitting devices', *Nature Nanotechnology*. Nature Publishing Group, 10(5), pp. 391–402. doi: 10.1038/nnano.2015.90.

Tauc J, Grigorovici, R. and Vancu, A. (1966) 'Optical Properties and Electronic Structure of Amorphous Germanium', *Physica Status Solidi (B)*, 15(2), pp. 627–637. doi: 10.1002/pssb.19660150224.

Thommes, M., Kaneko, K., Neimark, A. V., Olivier, J. P., Rodriguez-Reinoso, F., Rouquerol, J., and Sing, K. S. W. (2015) 'Physisorption of gases, with special reference to the evaluation of surface area and pore size distribution (IUPAC Technical Report)', *Pure and Applied Chemistry*, 87(9–10), pp. 1051–1069. doi: 10.1515/pac-2014-1117.

Tryba, B. (2008) 'Increase of the photocatalytic activity of TiO2 by carbon and iron modifications', *International Journal of Photoenergy*, 2008. doi: 10.1155/2008/721824.

UNESCO (2015) *Drops of Water, United Nations Educational, Scientific and Cultural Organization*. Available at: http://www.unesco.org/new/en/venice/special-themes/h2ooooh-initiative/h2ooooh-initiative-drops-of-water/ (Accessed: 12 May 2017).

Velasco, L. F. (2012b) *Fotodegradación oxidativa de fenol con catalizadores TiO2-C. Análisis de la respuesta fotoquímica de la fase carbonosa*. PhD thesis Universidad de Oviedo.

Velasco, L. F., Fonseca, I. M., Parra, J. B., Lima, J. C., and Ania, C. O. (2012) 'Photochemical behaviour of activated carbons under UV irradiation', *Carbon*, 50(1), pp. 249–258. doi: 10.1016/j.carbon.2011.08.042.

Velasco, L. F., Maurino, V., Laurenti, E., Fonseca, I. M., Lima, J. C., and Ania, C. O. (2013) 'Photoinduced reactions occurring on activated carbons. A combined photooxidation and ESR study', *Applied Catalysis A: General*. Elsevier B.V., 452, pp. 1–8. doi: 10.1016/j.apcata.2012.11.033.

Velasco, L. F., Lima, J. C. and Ania, C. (2014) 'Visible-light photochemical activity of nanoporous carbons under monochromatic light', *Angewandte Chemie - International Edition*, 53(16), pp. 4146–4148. doi: 10.1002/anie.201400887.

Velasco, L. F., Parra, J. B. and Ania, C. O. (2010) 'Role of activated carbon features on the photocatalytic degradation of phenol', *Applied Surface Science*, 256(17), pp. 5254–5258. doi: 10.1016/j.apsusc.2009.12.113.

Walker, C. H., Sibly, R. M., Hopkin, S. P., and Peaka, D. B. (2012) *Principles of Ecotoxicology*. Fourth Edi. London: Taylor & Francis Inc.

Warren, B. E. and Bodenstein, P. (1965) 'The diffraction pattern of fine particle carbon blacks', *Acta Cryst.*, (18), pp. 282–286.

Waters, P. and Lloyd, D. (1985) 'Salt, pH and Temperature Dependencies of Growth and Bioluminescence of Three Species of Luminous Bacteria Analysed on Gradient Plates', *Microbiology*, 131(11), pp. 2865–2869. doi: 10.1099/00221287-131-11-2865.

Wells, P. G., Lee, K. and Blaise, C. (1998) *Microscale Testing in Aquatic Toxicology*. New York: CRC Press.

Whelminger (2014) *EUROSTAT: Total water abstraction, share of surface water abstraction, by activity, 2011*. Available at: http://ec.europa.eu/eurostat/statistics-explained/index.php?title=File:Total_water_abstraction,_share_of_surface_water_abstraction,_by_activity,_2011_(m^3_per_inhabitant;_%25).png&oldid=191640 (Accessed: 10 August 2017).

Wilson, W. (2016) 'Water- Energy Nexus', in *World Energy Outlook 2016*. doi: 10.1021/es903811p.

Wongsarivej, P. and Tongprem, P. (2009) 'Phenolic wastewater treatment using activated carbon in a three phase fluidized-bed reactor', *Engineering Journal*, 13(3), pp. 57–65. doi: 10.4186/ej.2009.13.3.57.

WWAP (2009) *The United Nations World Water Development Report 3: Water in a Changing World*. Paris: UNESCO; London: Earthscan.

WWAP (2015) *The United Nations World Water Development Report 2015: Water for a Sustainable World*. Paris. doi: 978-92-3-100071-3.

WWAP (2017) *The United Nations World Water Development Report 2017. Wastewater: The Untapped Resource*. Paris.

References

Zazo, J. A., Casas, J. A., Mohedano, A. F., and Rodríguez, J. J. (2006) 'Catalytic wet peroxide oxidation of phenol with a Fe/active carbon catalyst', *Applied Catalysis B: Environmental*, 65(3–4), pp. 261–268. doi: 10.1016/j.apcatb.2006.02.008.

7. Annex A

- Example of EC_{50} calculation -

Calculation of EC_{50} and microtox data treatment

The results presented in this annex were obtained using a *p*-benzoquinone solution of 0.26 mg/L initial concentration.

Table A7.1 - Calculation of *p*-benzoquinone concentration for cuvettes A and B

Initial concentration of *p*-benzoquinone (mg/L)	**0.26**				
	A1	**A2**	**A3**	**A4**	**A5**
V_{NaCl}(µL)	1000	1000	1000	1000	250
$V_{p\text{-benzoquinone}}$(µL)	0	1000	1000	1000	2500
$C_{p\text{-benzoquinone}}$(mg/L)	0	0.03	0.06	0.12	0.24
	B1	B2	B3	B4	B5
V_{NaCl}(µL)	1000	500	500	500	500
$V_{p\text{-benzoquinone}}$(µL)	0	500	500	500	500
$C_{p\text{-benzoquinone}}$(mg/L)	0	0.01	0.03	0.06	0.12

Table A7.2 - Data treatment calculations of *p*-benzoquinone for Microtox equipment

	C (mg/L)	**Log (C)**	**I (0)**	**I(5)**	**I(15)**	**BR(5)**	**BR(15)**	**Icorr(5)**	**Icorr(15)**	**γ (5)**	**γ (15)**	**Log(γ (5))**	**Log(γ (15))**
B1	0.00	n/a	96	67	63	0.70	0.66	63	59				
B2	0.01	-1.831	90	36	35	--	--	70	66	0.74	0.688	-0.128	-0.163
B3	0.03	-1.530	100	30	30	--	--	70	66	1.33	1.188	0.123	0.075
B4	0.06	-1.228	100	10	12	--	--	63	59	5.98	4.469	0.777	0.650
B5	0.12	-0.927	90	2	4	--	--	63	59	30.41	13.766	1.483	1.139

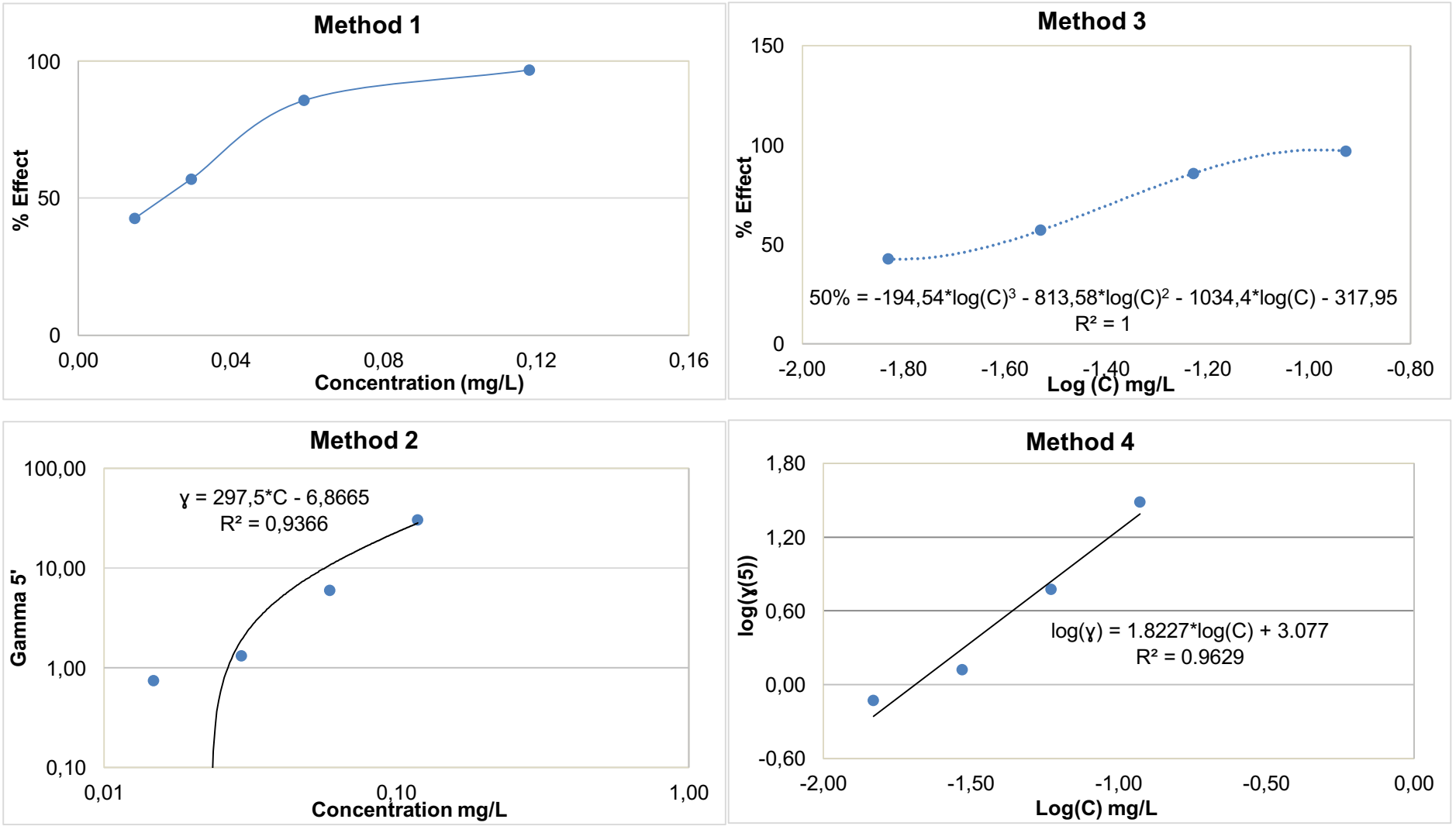

Figure A7.1 – Representation of the four methods used for the calculation of the EC50 value.

For all four methods, the main goal is to obtain 'C' – concentration in ppm – to calculate EC_{50}. Gamma value is considered '1' for the second and fourth methods.

Table A7.3 – EC50 average values for three repetitions using 4 different methods (green minimum and maximum values for EC_{50}-5' and in orange for EC_{50}-15').

Repetitions	R1	R2	R3	Average of repetitions (mg/L)
Method 1 (mg/L)				
EC_{50} 5'	0.022	0.023	0.026	0.024
EC_{50} 15'	0.024	0.023	0.030	0.025
Method 2 (mg/L)				
EC_{50} 5'	0.026	0.026	0.026	0.026
EC_{50} 15'	0.025	0.025	0.025	0.025
Method 3 (mg/L)				
EC_{50} 5'	0.024	0.023	0.027	0.025
EC_{50} 15'	0.026	0.023	0.029	0.026
Method 4 (mg/L)				
EC_{50} 5'	0.021	0.027	0.023	0.023
EC_{50} 15'	0.022	0.027	0.025	0.024

The same described methodology was used for calculation of all EC_{50} of the intermediates and phenol.

8. Annex B

- Individual plots of the industrial wastewater -

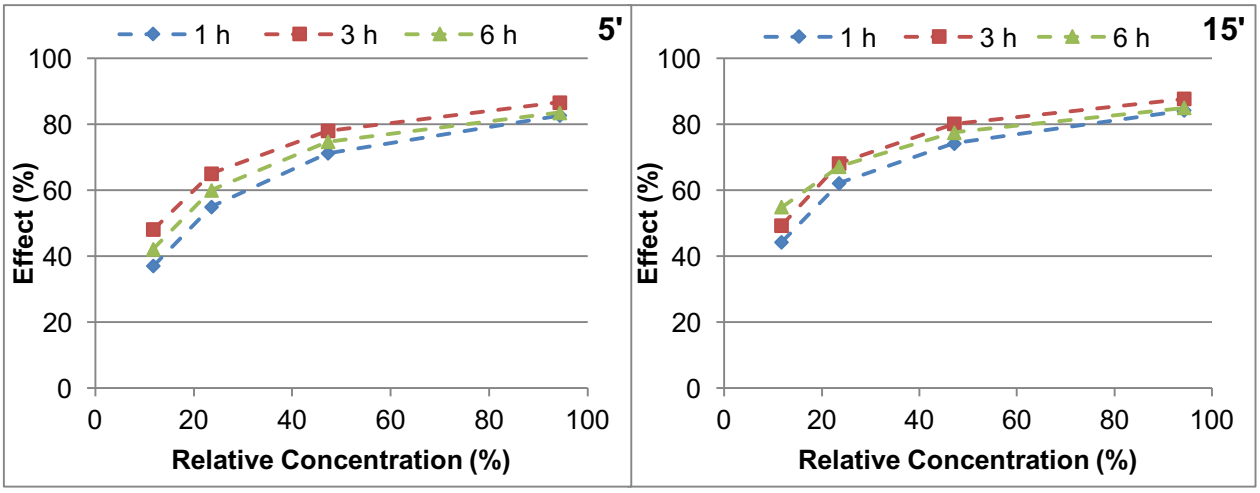

Figure A8.1 - Loss of bioluminescence signal after photolysis in 5' and 15' of incubation.

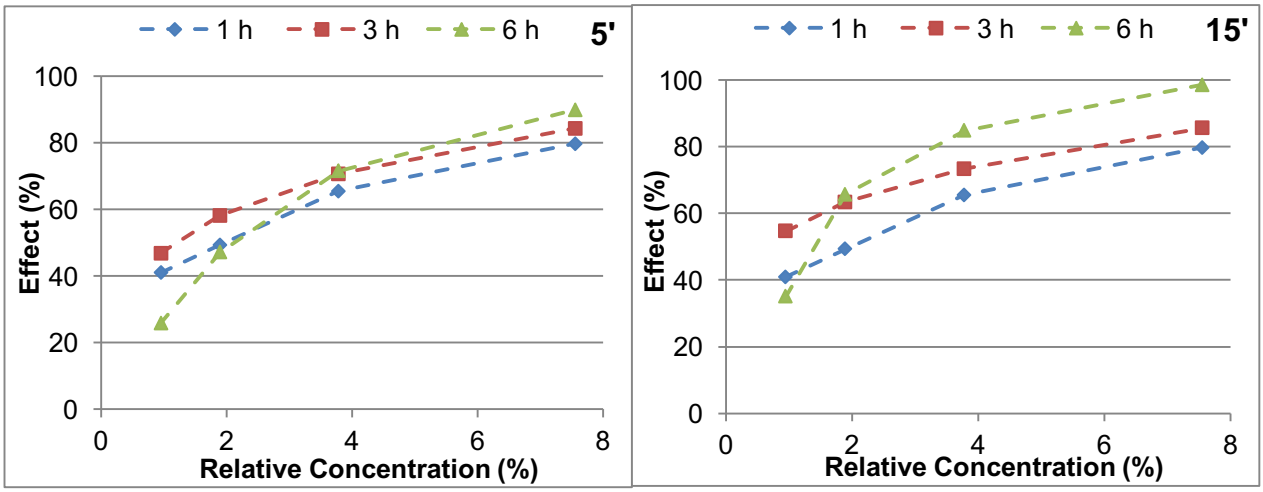

Figure A8.2 - Loss of bioluminescence signal after photocatalysis with TiO_2 in 5' and 15' of incubation.

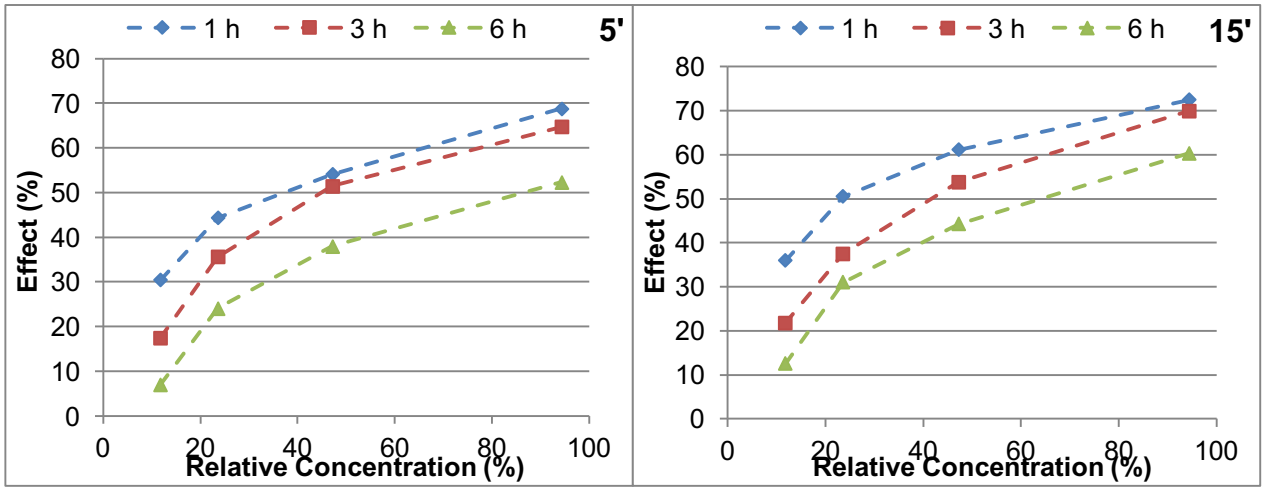

Figure A8.3 - Loss of bioluminescence signal after photocatalysis with CQ in 5' and 15' of incubation.

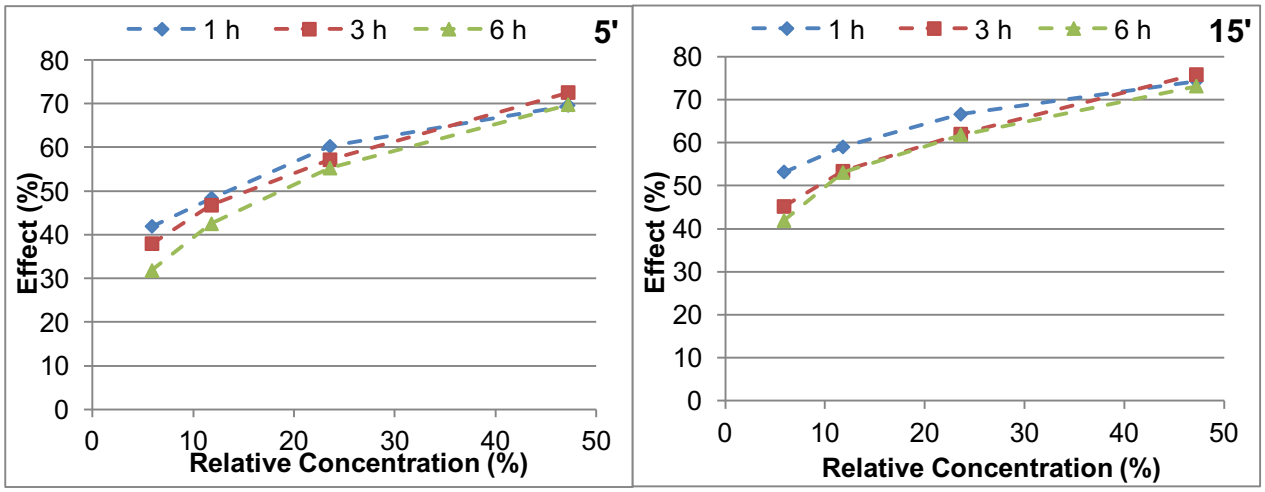

Figure A8.4 - Loss of bioluminescence signal after photocatalysis with TiO_2/CQ in 5' and 15' of incubation.